Quaternary Research

doi:10.1017/qua.2020.29

Reconstructing Mousterian landscapes in the southeastern Pyrenees (Roca dels Bous site, Pre-Pyrenees ranges, Spain)

Alfonso Benito-Calvo[a]*, Lee J. Arnold[b], Rafael Mora[c], Jorge Martínez-Moreno[c], Martina Demuro[b]

[a]Centro Nacional de Investigación sobre la Evolución Humana (CENIEH), Paseo Sierra de Atapuerca, 3, Burgos, Spain
[b]School of Physical Sciences, Environment Institute, and Institute for Photonics and Advanced Sensing (IPAS), University of Adelaide, North Terrace Campus, Adelaide, SA 5005, Australia
[c]Centre d'Estudis del Patrimoni Arqueològic de la Prehistoria (CEPAP-UAB), Universitat Autonoma de Barcelona, Bellaterra, Spain
*Corresponding author e-mail address: alfonso.benito@cenieh.es.

(Received December 6, 2019; Accepted March 18, 2020)

Abstract

Landscape evolution studies enable us to understand site formation processes affecting past hunter-gatherer settlements. This work presents a landscape reconstruction of Roca dels Bous site (RB), which is a reference site for the Late Mousterian occupation of the incised valleys of the southeastern Pyrenees. For this purpose, we combined geomorphological studies, stratigraphic descriptions, new single-grain optically stimulated luminescence datasets, statistical methods, and geophysical surveys. RB formed by gravitational processes induced by fluvial undermining of the Segre River during changing late Pleistocene climatic conditions. Geomorphological and chronological data combined with fluvial age-incision models suggest that, during Late Mousterian occupation, RB was located very near the Segre floodplain level and closer to water and raw material natural resources than at present. The accumulation of gravitational deposits associated with the archaeological levels occurred at rates of 0.16–0.44 m ka^{-1}, between 55 and 47 ka, coinciding with Marine Oxygen Isotope Stage 3 (MIS3). More detailed comparison with available climatic curves suggests that the dated RB layers were potentially deposited during cold phases within MIS3. This work provides new landscape-based evidence to examine the paleoenvironmental context of Neanderthal presence in the southeastern Pre-Pyrenees, an important region in the debate regarding Neanderthal demise in Western Europe around 40 ka.

Keywords: Landscape evolution; Roca dels Bous site; Mousterian; fluvial evolution; slope deposits; single-grain optically stimulated luminescence; MIS3

INTRODUCTION

Landform and geomorphic process reconstructions offer the opportunity to analyze the subsistence, settlement, and mobility of past hunter-gatherers across landscapes (Lazar and Schattner, 2010; Bailey and King, 2011; Reynolds et al., 2011). Base levels and topographic surfaces vary during landscape evolution, affecting site formation and changing the terrain, and therefore have physical and environmental significance (Benito-Calvo et al., 2008; 2017). Landscape stages also provide insights into the past distribution of natural resources (Wilson, 2011; Roy Sunyer et al., 2017) and the sequences of physical and environmental processes that affected settlement and land use strategies of past hominin populations.

In this study, we analyze the landscape evolution and formation processes that affected the Roca del Bous site (RB). This site constitutes a reference for the Late Mousterian occupations of the Iberian Peninsula and is located in the lowermost range of the southeastern Pyrenees, where several rock shelter sites reveal a recurrent landscape that appears to have been particularly attractive for Neanderthals during the late Pleistocene (Martínez-Moreno et al., 2004, 2010; Mora et al., 2011; Mora et al., 2014). In this area, the relief is characterized by narrow and incised valleys carved by the Segre River and its tributaries (Peña Monné, 1983; Lucha et al., 2012; Stange et al., 2013a), which provide natural corridors joining the lower and open plains of the Ebro Basin with the Pre-Pyrenees ranges. RB is a multi-layered Mousterian site located 35–36 m

Cite this article: Benito-Calvo, A., Arnold, L. J., Mora, R., Martínez-Moreno, J., Demuro, M. 2020. Reconstructing Mousterian landscapes in the southeastern Pyrenees (Roca dels Bous site, Pre-Pyrenees ranges, Spain). *Quaternary Research* 97, 167–186. https://doi.org/10.1017/qua.2020.29

above the Segre River, on a talus slope deposited at the foot of a large limestone cliff (Jordá Pardo et al., 1994; Jordá Pardo, 2005).

Formation of the RB site is investigated in this study by applying a multidisciplinary approach based on geomorphological, stratigraphical, geochronological, and geophysical methods. Specifically, geomorphological and stratigraphical studies, based on high resolution data (light detection and ranging [LIDAR] and unmanned aerial vehicle [UAV] surveys) and geophysical surveys, are combined with new single-grain optically stimulated luminescence (OSL) dating conducted on the archaeological levels of the site. These data are compared with a fluvial age-incision model estimated through statistical methods based on available published data for fluvial terraces. Using this combination of techniques, we are able to reconstruct the landscape and associated resources around RB, estimate the aggradation and incision rates affecting the landscape, and propose a correlation between the human occupations and the climatic events of the late Pleistocene.

GEOLOGICAL BACKGROUND

The RB site is located in the Paret de l´Ós cliff (Camarasa, Lleida, northwest Spain), around 35 m above the Segre River (Fig. 1). This area belongs to the Sierras Marginales range, which is an allochthonous and south-verging thrust and fold belt (Pocovi et al., 2004) found in the most external sector of the Pyrenees (Pre-Pyrenees). Geological formations in this area belong to the Triassic (Muschelkalk and Keuper units), Jurassic, Cretaceous, Cenozoic, and Quaternary (Fig. 1). Near the RB site, Cenozoic deposits consist of Eocene mudstones, Eocene conglomerates and limestones, and Oligocene conglomerates and shales (Saula i Briansó et al., 2017).

The Quaternary deposits around RB are mainly related to the Segre valley evolution. The Segre River is 265 km long and drains the largest catchment in the Southern Pyrenees, flowing from the Pyrenees Axial Zone until it joins the Ebro River in the Ebro Cenozoic basin. Quaternary evolution of the Segre valley has led to a fluvial terrace sequence mapped and studied in detail by several authors, who have collectively proposed a sequence composed mainly of seven fluvial terraces for different sectors of the Segre River (Peña Monné, 1983; Peña Monné and Sancho Marcen, 1988; Badía et al., 2009; Lucha, 2009; Lucha et al., 2012). More recently, Stange et al. (2013a) studied the complete Segre valley, compiling a sequence of seven terraces lying at + 113–100 m (TQ2), +88–77 m (TQ3), +65–48 m (TQ4), +47–35 m (TQ5), +28–16 m (TQ6), +14–8 m (TQ7) and + 5–3 m (TQ8) above the river. These terraces are 2–10 m thick and are composed of imbricated rounded and subrounded polymictic gravels (Roy Sunyer et al., 2017) that include lenticular levels of sands and silts. Terraces overlying the evaporate-cored Barbastro-Balaguer Anticline show abundant syn- and post-sedimentary gravitational deformation (Lucha, 2009; Lucha et al., 2012).

Recently, the middle and upper Segre terraces have been dated using the ^{10}Be exposure method, providing ages of 201.6 + 35.3/-32.9 ka for TQ9, 138.8 + 46.7/-22.8 ka for TQ10, 99.6 + 31.1/-19 ka for TQ11, and 61.8 + 4.6/-5.4 ka for TQ12 (Stange et al., 2013b). In other tributaries of the Segre River, such as the Noguera-Pallaresa valley, a terrace at + 15–25 m above the river bed and equivalent to level TQ13 has provided OSL ages between 23.5 ± 1.4 and 21.9 ± 1.3 ka (Roqué et al., 2013). In the Cinca valley, Lewis et al. (2009) proposed mean OSL ages of 178 ± 21 ka for a terrace at + 80 m, 97 ± 16 ka for a level lying at + 60 m, 61 ± 4 ka for a level at + 50 m, 47 ± 4 ka for a terrace at + 20 m (with outliers between 39 and 79 ka), and 11 ± 1 ka for a terrace at + 6–10 m. The oldest terrace in the Segre catchment has been dated at the Alcanadre valley (a tributary of the Cinca River), where Duval et al. (2015) and Sancho et al. (2016), provided electron spin resonance (ESR) ages of 1276 ± 104 ka and 817 ± 68 ka for levels situated, respectively, at relative elevations of + 180–200 m and + 120 m. However, in the other main catchment of the South Pyrenees, the Gállego River, fluvial terraces have provided older chronologies. In this valley, Benito et al. (2010), provided OSL ages between 133 ± 10 and 181 ± 13 ka for T9 (+30–50 m), between 124 ± 13 and 110 ± 20 ka for T10 (+20–30 m), between 55.4 ± 7.4 and 54.4 ± 8.8 ka for T11 (+10–12 m), and 16.8 ± 1.3 ka for T12 (+3–10 m).

Other Quaternary deposits in the area include alluvial cones, mantled pediments, karstic residual deposits (*terra rossa*), and gravitational landforms, such as the talus slope that contains the RB site (Jordá Pardo et al., 1994; Jordá Pardo, 2005; Benito-Calvo et al., 2009; Mora et al., 2014), or the talus flatirons documented in the Tremp depression (Roqué et al., 2013).

METHODS

Landscape reconstruction of the RB site is examined here through geomorphological, stratigraphical, geochronological, and geophysical methods. Geomorphological landforms were interpreted using fieldwork reconnaissance and several high-resolution spatial datasets (2 × 2 m LIDAR data, 0.25 m orthoimage from Plan Nacional de Ortofotografía Aerea [PNOA], http://pnoa.ign.es (20/04/2019); Figs. 2A and 3). Vertical geomorphological mapping of the Paret de l´Os cliff was performed using aerial photogrammetric surveys using UAV (Phantom 3 Pro) and Agisoft Metashape software (Figs. 2B and 3). Digital mapping tasks were carried out using the equipment available at the Digital Mapping and 3D Analysis Laboratory at the Centro Nacional de Investigación sobre la Evolución Humana (CENIEH).

In order to estimate the subsurface geometry of the talus slope where the RB site is located (Ortega et al., 2010), we applied the electrical resistivity tomography (ERT) geophysical method (Fig. 4, Table 1). We used pole-dipole arrays in order to achieve a greater surveying depth. Six ERT profiles were performed parallel and perpendicular

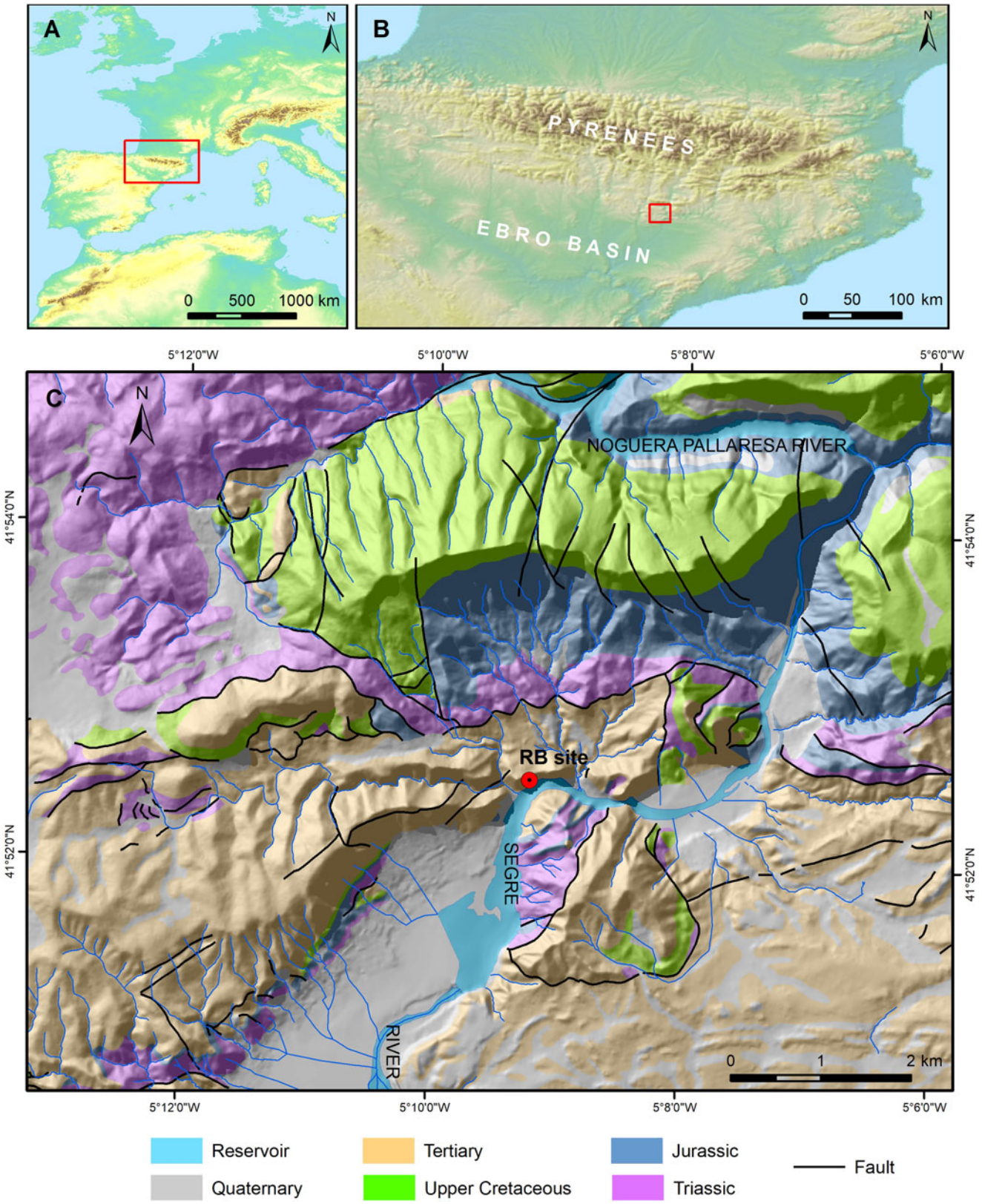

Figure 1. (color online) Geographical and geological setting of the Roca del Bous site.

to the cliff. ERT profiles were conducted by the surveying company Análisis y Gestión del Subsuelo using a Syscal resistivity meter.

Stratigraphic analysis of the RB site was carried out using field descriptions, and laboratory analysis focused on describing the texture and composition of fine sediment sub-samples.

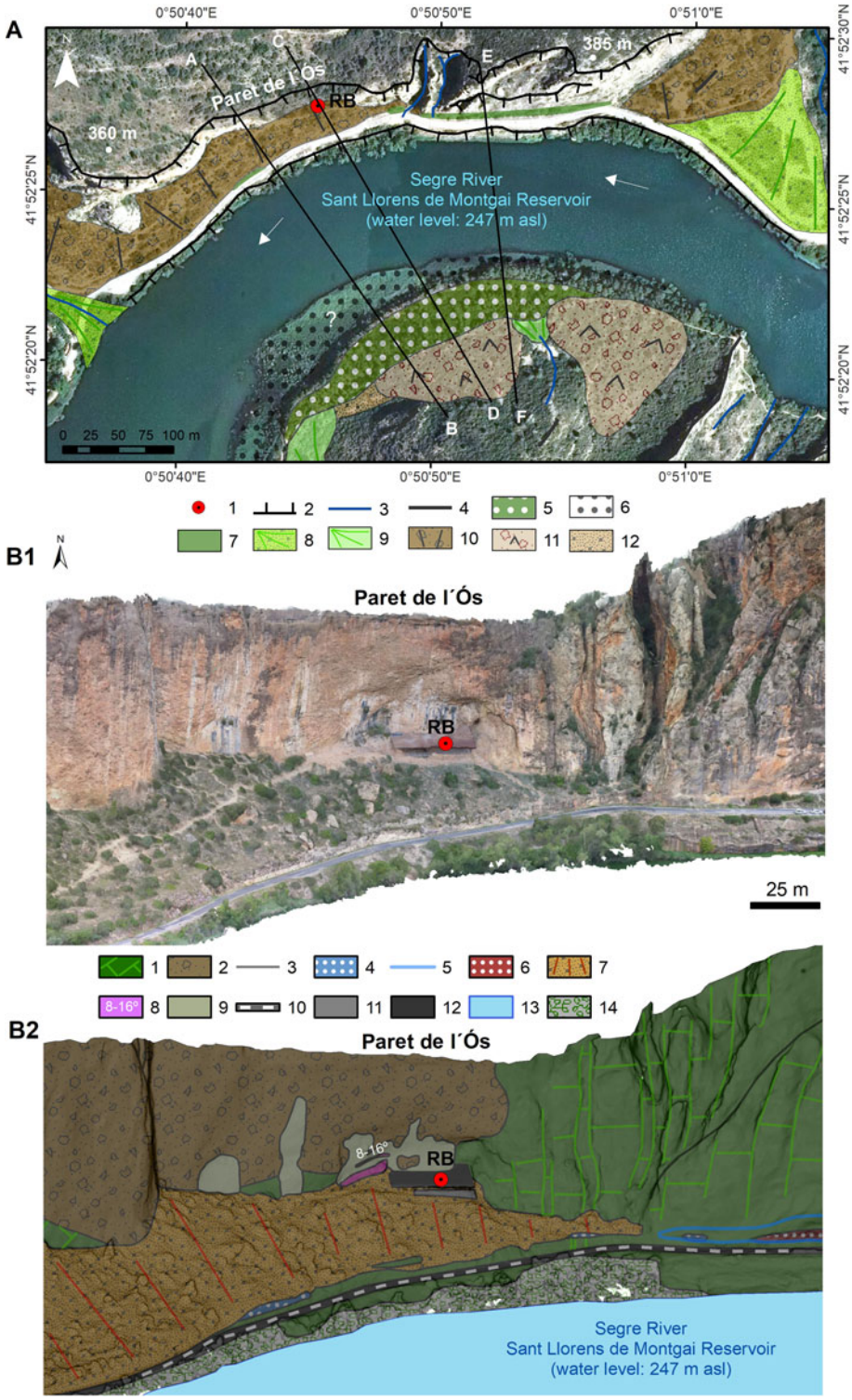

Figure 2. (color online) Geomorphological maps of the Segre meander and the Paret de l´Ós cliff where the Roca dels Bous (RB) site is located. (A) Geomorphological map of the Segre incised meander carried out using orthoimagery from Plan Nacional de Ortofotografía Aérea (PNOA), Instituto Geográfico Nacional (http://pnoa.ign.es/, 20/04/2019). Lettered lines show locations of the geomorphological cross-sections in Figure 3. Legend: 1, RB site; 2, scarps; 3, drainage network; 4, hogback lines; 5, fluvial terrace at + 7 m above the reservoir water level (254 m asl); 6, fluvial terrace semi-submerged by the reservoir; 7, fluvial terrace of the north margin (+10–16 m above the maximum water level of the reservoir); 8, hanging alluvial cone; 9, other cones; 10, talus slope; 11, landslides; 12, colluvium. (B1) Photogrammetric 3D model carried out using DJI Phantom drone and Leica GS15 GNSS. (B2) Geomorphological map of the Paret de l´Ós cliff. Legend: 1, Eocene limestones and lutites; 2, Oligocene conglomerates; 3, fractures and faults; 4, fluvial deposits of terrace at + 10–16 m above the reservoir water level; 5, groove carved on the limestone cliff; 6, fluvial and gravitational deposits; 7, talus slope deposits; 8, flowstone levels, with local dip; 9, seepage wall concretions; 10, road; 11, wall RB site; 12, RB site roof; 13, Sant Llorenç de Montgai Reservoir (maximum water level at 247 m asl); 14, vegetation.

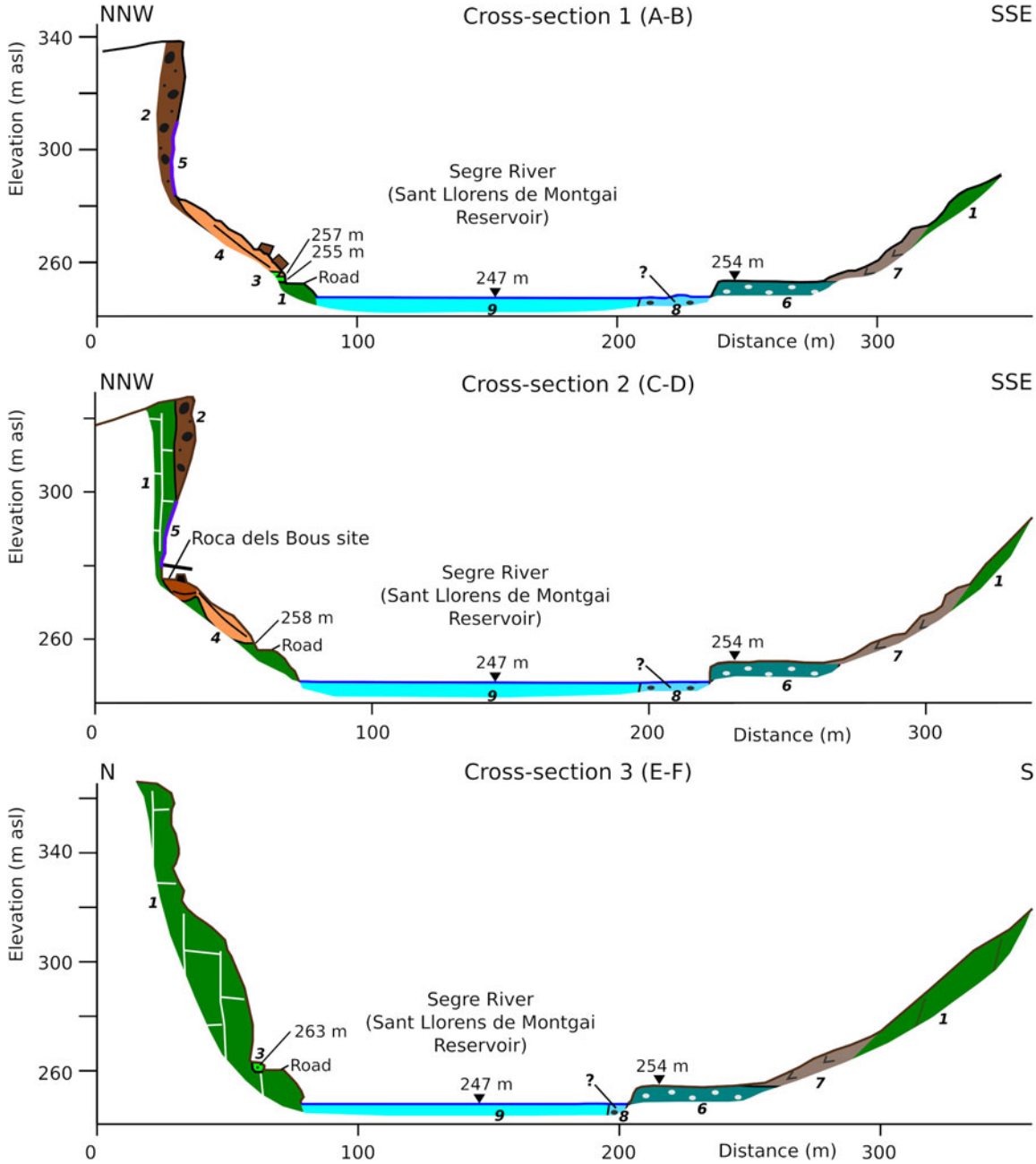

Figure 3. (color online) Geomorphological cross-sections of the incised meander and the aerial photogrammetric survey of the Paret de l´Ós cliff carried out using LIDAR data from Plan Nacional de Ortofotografía Aerea (PNOA, http://pnoa.ign.es, 20/04/2019). Legend: 1, Eocene limestones and lutites; 2, Oligocene conglomerates; 3, fluvial deposits of terrace at + 10–16 m above the reservoir water level, including gravitational deposits; 4, talus slope deposits; 5, seepage wall concretion; 6, fluvial terrace at + 7 m above the reservoir water level (254 m asl); 7, landslide; 8, fluvial terrace semi-submerged by the reservoir; 9, Sant Llorens de Montgai Reservoir (maximum water level at 247 m asl). See Figure 2A for position of cross-sections.

Particle size sieving and laser diffraction techniques were used for describing texture (Geology Laboratory, CENIEH), while X-ray diffraction was applied to determine qualitative mineralogical composition (Archaeometry Laboratory, CENIEH). Stratigraphical sections were mapped in ArcGIS from orthophotos georeferenced in the local excavation coordinate system using a total station (Fig. 5).

The chronology of the RB site has been determined using single-grain OSL dating of five sediment samples collected from stratigraphic units RB-G, RB-M, RB-N, and RB-O (Fig. 5, Table 2). The OSL samples were taken from cleaned exposure faces at nighttime or under light-proof sheeting using filtered red LED lighting and immediately sealed in opaque plastic containers upon extraction. Quartz grains were processed under safe (dim red) light conditions at the CENIEH luminescence dating facility (Burgos, Spain) using standard preparation procedures (e.g., Demuro et al., 2013), including a 48% hydrofluoric acid etch (40 minutes)

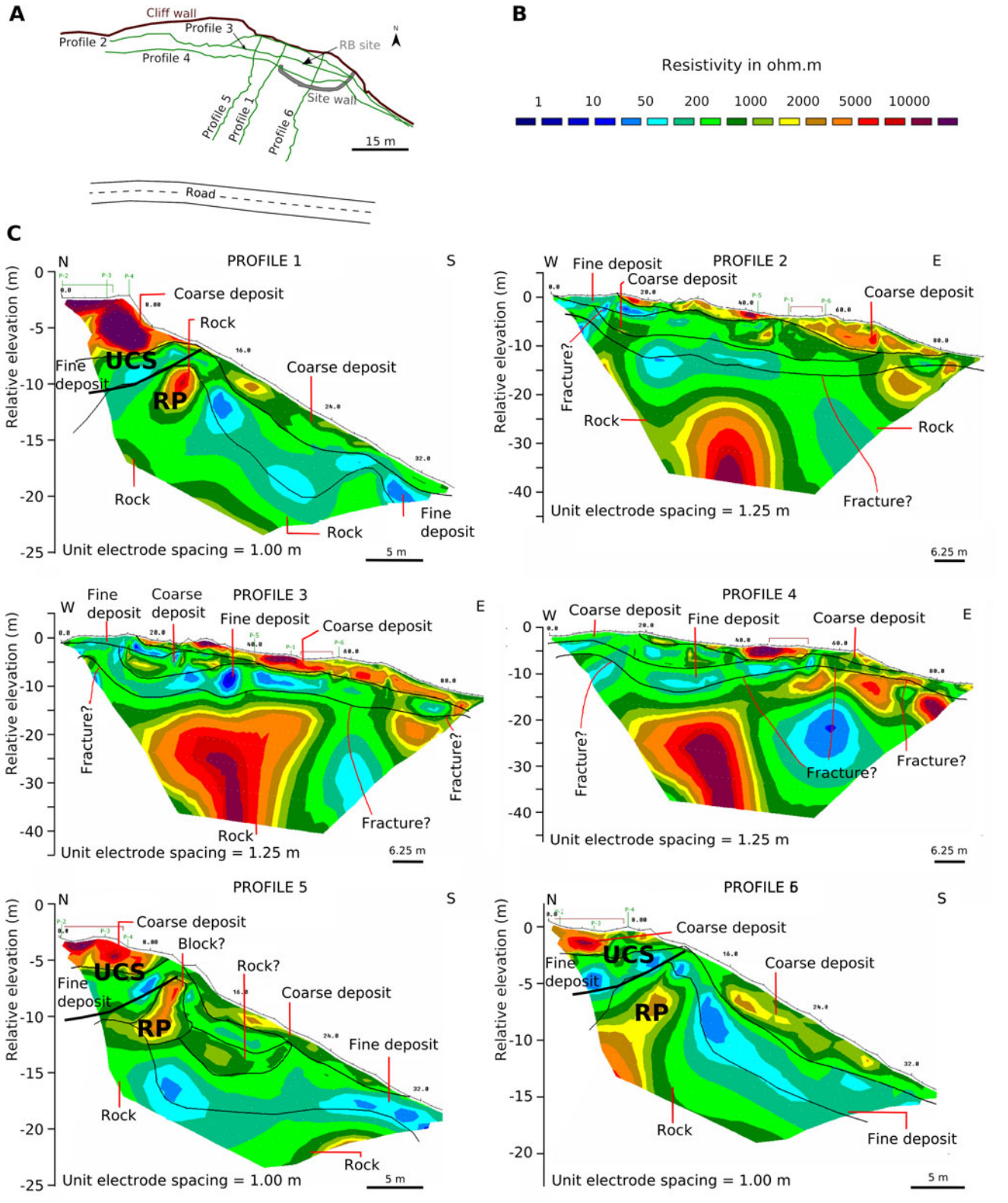

Figure 4. (color online) Electrical resistivity tomography (ERT) analysis of the talus slope in the Roca dels Bous site. (A) Profile locations. (B) Standardized resistivity color scale. (C) ERT profiles using Schlumberger-Wenner and Pole-Dipole arrays. UCS, Upper concave-up accommodation space; RP, Rocky projection.

Table 1. Technical characteristics of the electrical resistivity tomography profiles carried out in the Roca dels Bous site.

Profiles	Characteristics			
	Length (m)	*Number of electrodes*	*Gap (m)*	*Depth (m)*
SANT-1	35	36	1	13
SANT-2	88.75	72	1.25	36
SANT-3	88.75	72	1.25	36
SANT-4	88.75	72	1.25	36
SANT-5	35	36	1	13
SANT-6	35	36	1	13

to remove the alpha-irradiated outer layers of the quartz extracts. OSL measurements were made using the experimental apparatus described by Arnold et al. (2013, 2016). For equivalent dose (D_e) evaluation, quartz grains with a diameter of 212–250 µm were measured in aluminum discs drilled with an array of 300 × 300 µm holes to ensure true single-grain resolution (Arnold et al., 2012b). Individual D_e values were determined using the single-aliquot regenerative-dose (SAR) procedure (Murray and Wintle, 2000) shown in Supplementary Table S1, which yielded suitable multi-grain aliquot and single-grain dose recovery test results for sample RB12-1 (Fig. 6A, Supplementary Table S1). Between 1000 and 1100 single-grain D_e measurements were made for each sample (Supplementary Table S2); individual D_e values were included in the final age calculation if they satisfied a series of standard and widely tested quality-assurance criteria, as detailed in Arnold et al. (2013, 2016). Sensitivity-corrected dose-response curves were constructed using the first 0.08 s of each OSL stimulation after subtracting a mean background count obtained from the last 0.25 s of the signal (Supplementary Fig. S2). The environmental dose rate for the RB OSL samples was estimated using a combination of in situ field gamma spectrometry and low-level beta counting, taking into account cosmic ray contributions (Prescott and Hutton, 1994), an assumed minor internal alpha dose rate (Bowler et al., 2003), beta-dose attenuation, and long-term water content, as detailed in Table 2. Further details of the OSL dating procedures are provided in the Supplementary Information.

OSL ages are presented throughout this study with their 1σ uncertainty ranges, in accordance with standard OSL dating reporting conventions (e.g., Duller, 2008; Arnold and Demuro, 2018). As detailed in Table 2 and the Supplementary Information, the OSL dating 1σ uncertainty ranges incorporate random measurement and fitting uncertainties, systematic uncertainties on instrument calibration and conversion factors, and indirectly quantified uncertainties on burial history and dose-rate parameters.

The RB OSL results obtained in this study and fluvial terrace data were used to compare the empirical chronology and position of the RB site with a general age-incision model of the Segre River (Fig. 7). These kinds of models reconstruct the mean incision history of valleys by applying regression curves to the terrace ages and the relative elevations of the terrace treads (Silva et al., 2013 and 2016). The model was carried out using polynomial and power functions (Fig. 7A), considering two cases: the maximum and the minimum relative tread elevations proposed for the dated terraces (Stange et al., 2013a, 2013b). In this work, we test polynomial and power functions obtaining R-squared of 99% and 98%, respectively.

RESULTS

Geomorphology

The RB site is a shallow rock shelter developed at the foot of a west-northwest–east-southeast cliff (Paret de l´Ós), which is situated on the outer bank of an incised meander of the Segre River (Fig. 2A; Benito-Calvo et al., 2009). This cliff has largely been formed following erosion of the Eocene bioclastic limestones and the Oligocene conglomerates (Fig. 2B).

In the central and western sectors, the cliff base includes a talus slope (slope: 29–32°, maximum height: 289 m asl) composed of loose and heterometric scree (including metric boulders), eroded from the cliff (Fig. 2B). In the RB area, the talus slope is capped by a unit of flowstones (Jordá Pardo et al., 1994; Jordá Pardo, 2005; Benito-Calvo et al., 2009), consisting of two main phases of subhorizontal and recrystallized flowstones sloping 8–16° towards the southwest. The upper level is highly eroded, consisting of a 0.6 cm-thick flowstone layer cementing debris deposits, which is currently hanging, attached to the cliff; 1.4 m below this level, another flowstone phase >1 m thick lies on the upper part of the preserved talus slopes (Fig. 2B2). Subhorizontal flowstones are found below seepages, whose source is located at the contact between the conglomerates and the limestones.

Talus slope deposits lie on Eocene limestones and, locally, on rounded and subrounded imbricated gravels at 257–263 m asl (Figs. 2 and 3). These fluvial deposits were considered to be older than all of the talus slope deposits (Jordá Pardo et al., 1994; Jordá Pardo, 2005; Mora et al., 2014). Nevertheless, angular boulders can also be observed embedded in the fluvial deposits (Jordá Pardo et al., 1994), indicating gravitational degradation of the cliff during the fluvial sedimentation episode. Towards the east-northeast, the base of the limestone cliff is carved by a subhorizontal groove containing fluvial gravels, sands, and silts and including gravitational limestone blocks and fragments. This groove is located at + 16 m above the reservoir water level (awl) and would have formed by fluvio-karstic processes undermining the cliff (Guerrero and Gutiérrez, 2017).

Altogether, the top of the fluvial deposits preserved on the steep northern margin of the Segre valley reach + 16 m above the maximum water level of the Sant Llorenç de Montgai reservoir (maximum water level: 247 m asl, Confederación Hidrográfica del Ebro, 2019) and seem to belong to the same fluvial terrace level. In contrast, the southern margin

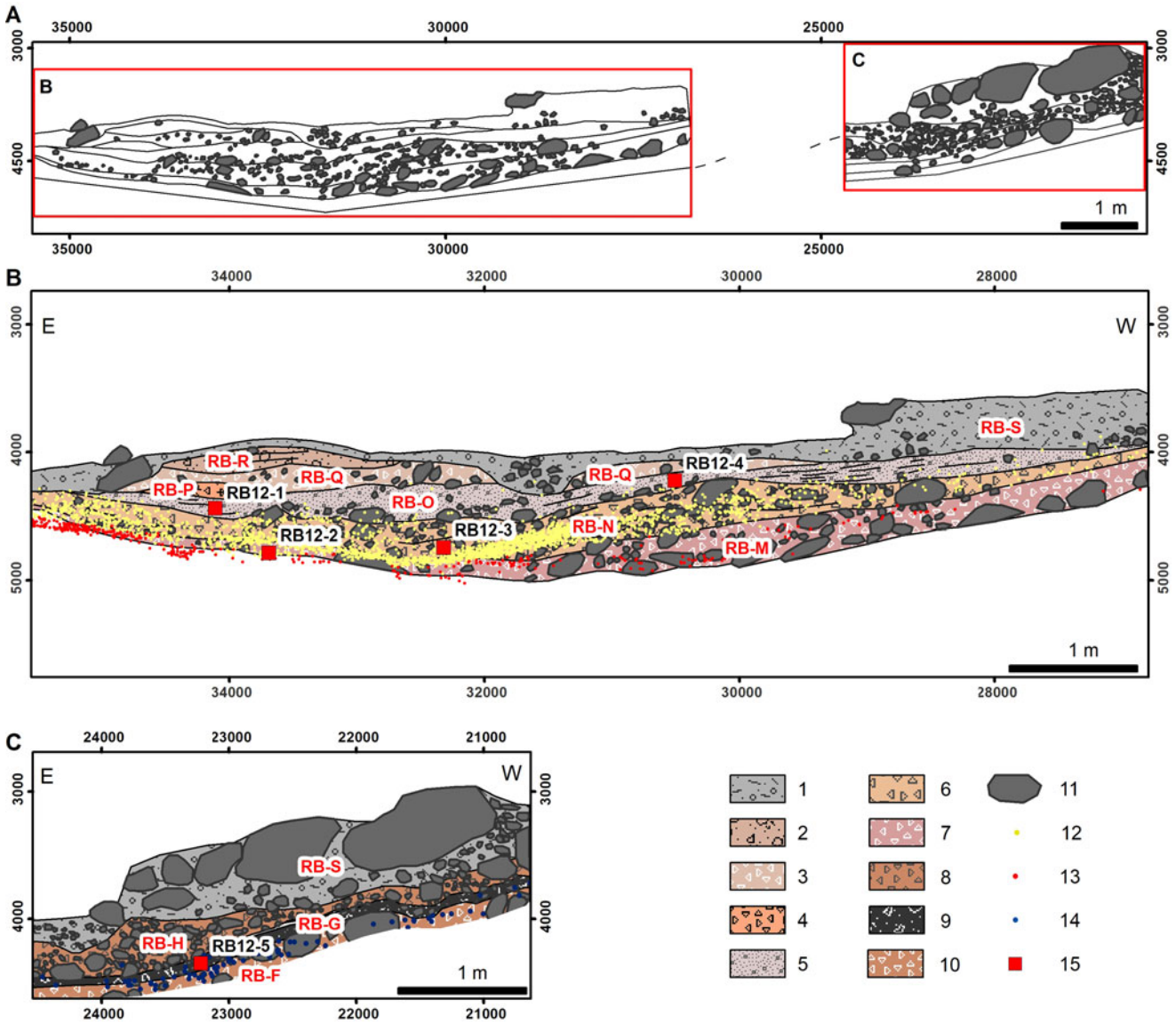

Figure 5. (color online) Stratigraphic sections of the Roca dels Bous (RB) site, digitalized in GIS from orthophotos georeferenced with a total station. Local cartesian coordinate system in mm. (A) E–W general section. (B) Sequence of the eastern and central areas. (C) Sequence of the western sector. Legend: 1, recent anthropic layer (RB-S); 2, coarse-bedded fining-upward angular pebbles, includes a pale yellow silty sandy matrix (RB-R) and the archaeological level N10; 3, angular and sub-angular coarse pebbles, scarce cobbles, and massive sands (RB-Q); 4, lens of moderately sorted sub-angular to sub-rounded medium pebbles with reddish sandy mud matrix (RB-P); 5, massive grey sands to the east, locally laminated and concreted, and bedded pebbles to the west (RB-O); 6, angular and sub-angular very coarse pebbles and some cobbles, showing fining-upward cycles (RB-N), contains archaeological level N12; 7, angular and sub-angular coarse to fine pebbles with grey sandy mud matrix (RB-M), contains archaeological level N14; 8, angular and sub-angular cobbles and very coarse pebbles with scarce red-brown sandy mud matrix (RB-H); 9, combustion ashes (RB-G); 10; angular pebbles, cobbles, and blocks with large interparticle voids and scarce sandy mud matrix (RB-F); 11, angular boulders and cobbles; 12, archaeological level N12; 13, archaeological level N14; 14, archaeological level S9; 15, OSL samples.

of the valley contains two lower terraces, with treads at +7 m awl, that are semi-submerged by the reservoir water level (Figs. 2 and 3).

Thus, RB site is located in an asymmetric incised meander with terrace levels at + 16 m, +7 m, and approximately + 0 m awl. Considering (1) the relative elevations of the identified terraces above the reservoir water level, (2) the mean depth of the reservoir (7.6 m, Confederación Hidrográfica del Ebro, 2019), and (3) the position of the study area at the tail of the reservoir, where the water depth should be around 3–4 m, we infer that these three terraces would correspond, respectively, to the Segre terrace levels TQ14 (+16–28 m), TQ15 (+8–14 m), and TQ16 (+3–5 m), which have been mapped downstream and upstream of the incised meander (Peña Monné, 1983; Badía et al., 2009; Lucha, 2009; Lucha et al., 2012; Roqué et al., 2013; Stange et al., 2013a). These terraces lie 16, 25, and 32 m below the RB excavation, respectively.

Table 2. Dose rate data, single-grain equivalent doses, and quartz optically stimulated luminescence (OSL) ages for the Roca dels Bous (RB) samples.

				Environmental dose rate (Gy/ka)				Equivalent dose (D_e) data				
Sample name	Level	Grain size (μm)	Water content[a]	Beta dose rate[b,c]	Gamma dose rate[c,d]	Cosmic dose rate[e]	Total dose rate[c, f,g]	No. of grains[h]	Over-dispersion (%)[i]	Age model[j,k]	D_e (Gy)[f]	OSL age (ka)[f,l]
RB12-1	RB-O	212–250	18 ± 4	1.23 ± 0.06	0.61 ± 0.02	0.04 ± 0.01	1.91 ± 0.11	97 / 1100	35 ± 4	MAM-3	90 ± 5	47.0 ± 4.0
RB12-4	RB-O	212–250	18 ± 4	1.33 ± 0.06	0.60 ± 0.02	0.04 ± 0.01	2.00 ± 0.11	91 / 1000	34 ± 4	MAM-3	97 ± 6	48.5 ± 4.2
RB12-3	RB-N	212–250	21 ± 4	1.24 ± 0.06	0.41 ± 0.02	0.04 ± 0.01	1.72 ± 0.11	128 / 1100	46 ± 4	MAM-4	83 ± 6	48.4 ± 4.7
RB12-2	RB-M	212–250	14 ± 3	1.11 ± 0.05	0.46 ± 0.02	0.04 ± 0.01	1.64 ± 0.08	108 / 1000	37 ± 4	MAM-3	80 ± 6	48.8 ± 4.4
RB12-5	RB-G	212–250	14 ± 3	0.91 ± 0.04	0.30 ± 0.01	0.04 ± 0.01	1.28 ± 0.07	135 / 1000	43 ± 3	MAM-3	71 ± 6	55.2 ± 5.5

[a]Long-term water content, expressed as % of dry mass of mineral fraction, with an assigned relative uncertainty of ± 20%. The present-day water contents of these samples (1–2% of dry weight) are not considered to be representative of those prevailing throughout the sample burial periods, as the excavation pits and sediment exposures had partially dried out prior to sampling. Long-term water contents have therefore been calculated as being equivalent to 60% of the present-day saturated water values on the basis of proportional saturation assessments made in similar depositional and climatic contexts across the Iberian Peninsula (e.g., Arnold et al., 2013, 2014, 2015; Demuro et al., 2019a, 2019b).

[b]Beta dose rates were calculated on dried and powdered sediment samples using a Risø GM-25-5 low-level beta counter (Bøtter-Jensen and Mejdahl, 1988), after making allowance for beta dose attenuation due to grain-size effects and hydrofluoric acid etching (Brennan, 2003).

[c]Specific activities and radionuclide concentrations have been converted to dose rates using the conversion factors given in Guérin et al. (2011), making allowance for beta-dose attenuation (Mejdahl, 1979; Brennan, 2003).

[d]Gamma dose rates were calculated from in situ measurements made at each sample position with a NaI:Tl detector, using the "energy windows" approach (e.g., Arnold et al., 2012a).

[e]Cosmic-ray dose rates were calculated using the approach of Prescott and Hutton (1994) and assigned a relative uncertainty of ± 10%.

[f]Mean ± total uncertainty (68% confidence interval), calculated as the quadratic sum of the random and systematic uncertainties.

[g]Includes an internal dose rate of 0.03 Gy/ka with an assigned relative uncertainty of ± 30%, based on intrinsic ^{238}U and ^{232}Th contents published by Mejdahl (1987), Bowler et al. (2003), Jacobs et al. (2006), and Pawleyet al. (2008), and an a-value of 0.04 ± 0.01 (Rees-Jones, 1995; Rees-Jones and Tite, 1997).

[h]Number of D_e measurements that passed the single-aliquot regenerative-dose rejection criteria and were used for D_e determination / total number of grains analyzed.

[i]The relative spread in the D_e dataset beyond that associated with the measurement uncertainties of individual D_e values, calculated using the central age model of Galbraith et al. (1999).

[j]Age model used to calculate the sample-averaged D_e value for each sample. MAM-3 = 3-parameter minimum age model of Galbraith et al. (1999). MAM-4 = 4-parameter minimum age model of Galbraith et al. (1999). MAM-3 and MAM-4 D_e estimates were calculated after adding, in quadrature, a relative error of 10% to each individual D_e measurement error to approximate the underlying dose overdispersion observed in the single-grain dose-recovery test for sample RB12-1.

[k]Age model selection: The RB samples are interpreted as being heterogeneously bleached on the basis of their D_e distribution characteristics, high overdispersion values, and complex geomorphic contexts (see main text for further discussion). The choice of whether to use the MAM-3 or MAM-4 for each sample was made on statistical grounds using the maximum log likelihood score criterion outlined by Arnold et al. (2009).

[l]Total uncertainty includes a systematic component of ± 2% associated with laboratory beta-source calibration.

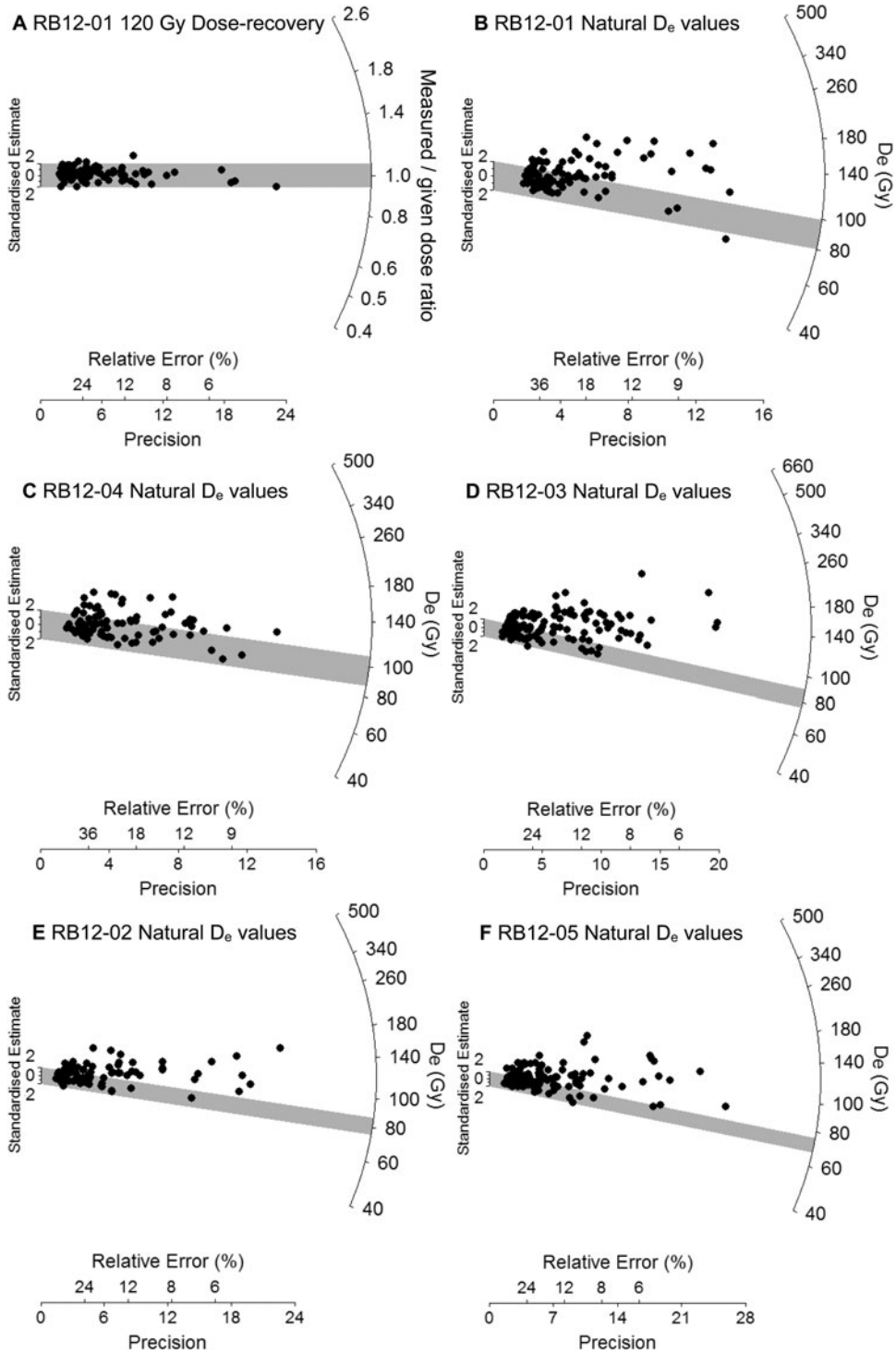

Figure 6. Single-grain optically stimulated luminescence (OSL) D_e distributions for the Roca dels Bous (RB) samples, shown as radial plots. (A) Measured to given dose ratios obtained for individual quartz grains of sample RB12-01 in the single-aliquot regenerative-dose recovery test. The gray-shaded region is centered on the administered dose for each grain (sample average = 120 Gy). Individual D_e values that fall within the shaded region are consistent with the administered dose at 2σ. (B)–(F) Natural single-grain D_e datasets for the five OSL samples dated in this study. The gray bands are centered on the D_e values used for the age calculations, which were derived using either the 3-parameter MAM (samples RB12-1, RB12-2, RB12-4, and RB12-5) or the 4-parameter MAM (sample RB12-3) of Galbraith et al. (1999).

ERT survey

Six ERT profiles were carried out; their distributions, resistivity values, and interpretations are shown in Figure 4. The ERT profiles define a surficial level of high resistivity interpreted as coarse debris with no or very scarce matrix located in the first 3–5 m. These deposits correspond to the archaeological levels that are currently being excavated at RB. Below this high

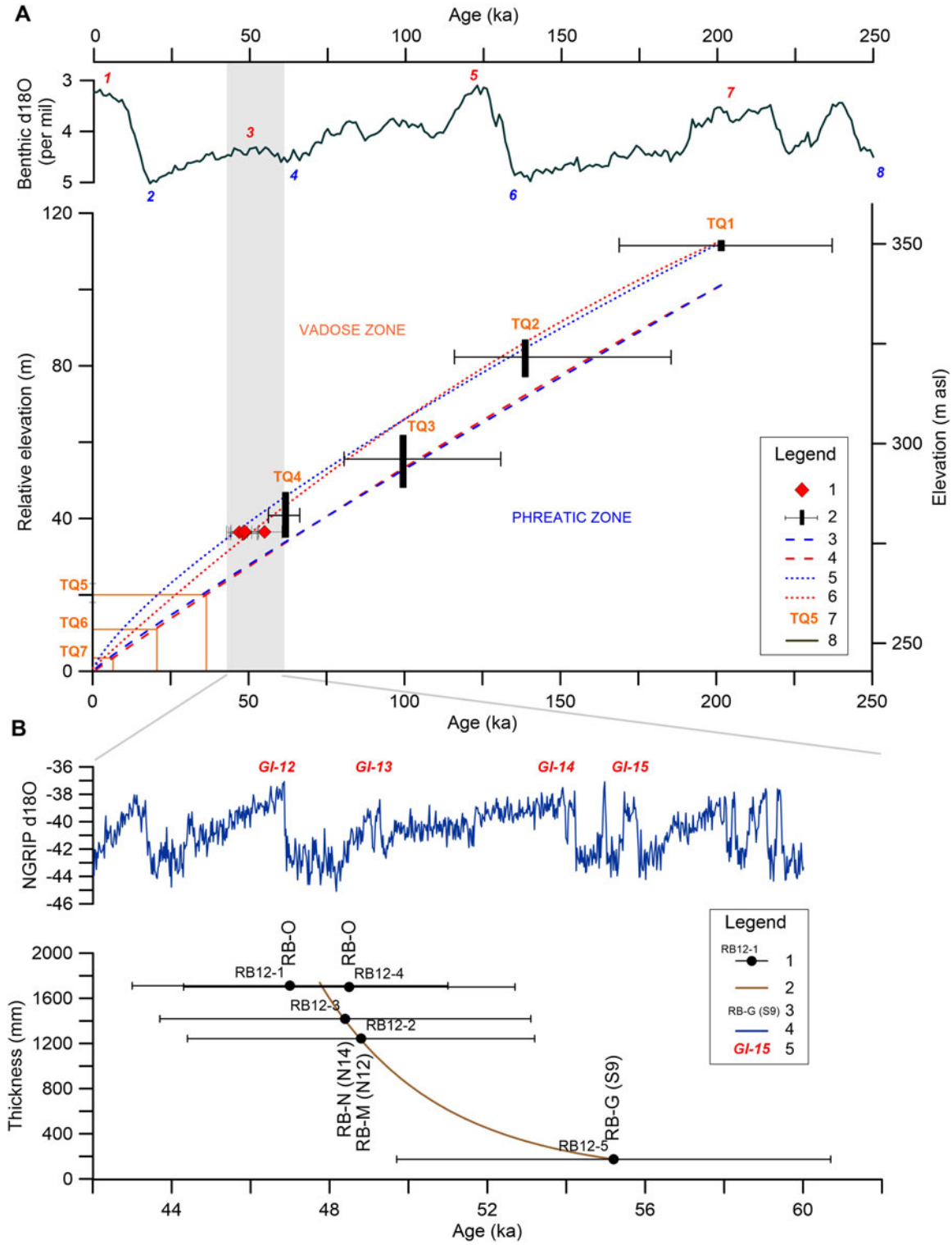

Figure 7. (color online) (A) Segre age-incision model and position of Roca dels Bous (RB) layers. Legend: 1, RB optically stimulated luminescence (OSL) ages (this study); 2, Segre River terrace exposure ages and tread relative elevation (Stange et al., 2013a, 2013b); 3, power regression model using ages and minimum tread terrace elevation (R2 = 0.98); 4, polynomial regression model using ages and minimum tread terrace elevation (R2 = 0.99); 5, power regression model using ages and maximum tread terrace elevation (R^2 = 0.98); 6, polynomial regression model using ages and maximum tread terrace elevation (R^2 = 0.99); 7, terrace fluvial deposits located beneath RB site, at + 10–16 m above the reservoir water level; 8, marine isotopic curve (Lisiecki and Raymo, 2005). (B) Correlation of RB units and archaeological levels with the MIS3 isotopic curve. Legend: 1, RB OSL ages and associated 1σ uncertainty ranges; 2, general aggradation model (Power function, R^2 = 99%); 3, stratigraphic and archaeological level; 4, GICC05 isotopic curve (Svensson et al., 2008); 5, glacial interstadials (GI) (Svensson et al., 2008).

resistivity area lies a 2–6 m-thick high-conductivity area, likely associated with a deposit that includes abundant clays, silts, or sands. Underlying the high-conductivity area, another high-resistivity level is found, interpreted as the bedrock. In addition to these three resistivity layers, we identified vertical and sub-vertical structures with low resistivity values, which are potentially explained as fractures that mainly affect the bedrock.

Stratigraphy

The RB site is located towards the top of the talus slope, in the debris deposits located 9 m below the sub-horizontal flowstone unit that caps the sequence (Jordá Pardo et al., 1994; Jordá Pardo, 2005). The archaeological excavation carried out between 2001 and 2018 over an area of 100 square m has exposed a 2.5-m-thick sequence of undisturbed deposits (Fig. 5). The latter shows a smoothly concave-up structure, which is recognizable both in the N–S and E–W directions (Figs. 4 and 5). In the E–W direction, this structure has been explained by the coalescence of two talus cones that converge in the site (Mora et al., 2014). The excavated sequence is composed primarily of unconsolidated pebble- to boulder-sized breccias (Benito-Calvo et al., 2009), mainly clast-supported and locally matrix-supported, very poorly sorted to moderately sorted, showing massive structure or local discontinuous and sub-parallel bedding (Fig. 5). In some layers, homometric clasts (layers RB-R, RB-Q, and RB-P) and local cycles of fining-upward sequences are recognizable (layer RB-N). Large clasts are more abundant in layers RB-M, RB-H, and RB-F, where centimetric interparticle voids are common. The clasts in these layers are composed of Eocene limestones and Oligocene conglomerates, while the matrix displays a sandy mud texture (sands: 39–50%, muds: 50–60%), massive structure, and gray, brown, and red colors. Layer RB-Q includes a sand layer at the top, while unit RB-O shows a succession of gray sands, locally laminated, including laminar carbonate concretions towards the top. Matrix and sand deposits are dominated by quartz and calcite, and to a lesser degree, phyllosilicates, plagioclase, K-feldspar, and iron oxides.

In this sequence, late Pleistocene sediments of anthropic origin also appear. Between layers RB-H and RB-F, a combustion ash layer emerges (RB-G), which is related to archaeological level S9. Additionally, several hearths and artifacts made of quartzite and flint have been excavated and collected from archaeological levels N10, N12, and N14, which are contained within stratigraphical layers RB-R, RB-N, and RB-M, respectively (Martínez-Moreno et al., 2016) (Fig. 5). The fabric analysis conducted on the artifacts of level N12 reveals a planar fabric characterized by a higher isotropic component than the fabric of the natural clasts contained in the same stratigraphical unit RB-N (Benito-Calvo et al., 2009).

Single-grain OSL chronology

Table 2 provides a summary of the environmental dose rates, D_e values, and final ages obtained for the five OSL dating samples. Between 9 and 13% of quartz grains measured per sample were considered suitable for OSL dating purposes after application of the SAR quality assurance criteria (Supplementary Table S2). The single-grain D_e distribution of each sample is shown as a radial plot in Figure 6.

All five of the RB OSL samples exhibit relatively heterogeneous D_e distributions, characterized by a large proportion of measured D_e values lying outside of the weighted mean burial dose 2σ ranges, and distinct leading-edges of low D_e values or tails of higher D_e values (Fig. 6). The overdispersion values for these samples range between 34 and 46% (Table 2), which are higher than those typically reported for ideal (well-bleached and unmixed) single-grain D_e datasets at 2σ (e.g., the global average reported by Arnold and Roberts [2009] = 20 ± 1%) and significantly higher than the overdispersion value of 6 ± 3% obtained for the single-grain dose recovery test of sample RB12-1. Collectively, these D_e distribution characteristics suggest that dose dispersion originating from extrinsic, field-related sources, and/or intrinsic experimental sources not captured by the dose recovery test, have exerted a significant influence on the RB samples.

In attempting to ascertain the dominant sources of additional D_e scatter, it is important to take into consideration the sediment transportation and deposition dynamics of the RB sediments. The OSL samples collected from this site contain a significant component of locally derived colluvial (talus slope) deposits that are likely to have experienced limited transportation distances and daylight exposure prior to their accumulation within the rock shelter. The sediment matrix is also likely to include minor populations of autochthonous quartz grains derived directly from the spallation of exposed bedrock surfaces or in situ weathering of gravitationally transported clasts that accumulated alongside externally derived, well-bleached grain populations. Given the potentially complex depositional context of the RB site, which is dominated by locally derived gravitational processes, it seems feasible that the additional D_e scatter observed for the OSL samples may be primarily attributable to heterogeneous bleaching at the time of deposition (e.g., Olley et al., 1999, 2004; Bailey and Arnold, 2006; Arnold et al., 2007, 2008, 2009); however, minor dose dispersion arising from intrinsic sources of D_e scatter (e.g., Demuro et al., 2013) or spatial variations in beta dose rates experienced by individual grains (e.g., Nathan et al., 2003; Mayya et al., 2006) cannot necessarily be discounted in this depositional context. Post-depositional mixing or bioturbation (e.g., Roberts et al., 1998; Arnold et al., 2009, 2013) are not, however, thought to have contributed significantly to the heterogeneous D_e datasets observed at RB given the preservation of clear stratigraphic layering and laterally continuous archaeological horizons (Fig. 5).

On the basis of these D_e interpretations, we have opted to use the minimum age model (MAM) to derive the burial dose estimates for the RB OSL samples (Table 2). The decision of whether to use the three parameter or four parameter model (MAM-3 or MAM-4) for the final age calculation of each sample has been made on statistical grounds using the

maximum log likelihood score outlined by Arnold et al. (2009). The final OSL ages shown in Table 2 are stratigraphically consistent through the RB sequence when considering the associated 1σ uncertainty ranges and indicate that horizons RB-O to RB-G accumulated between 47.0 ± 4 ka and 55.2 ± 5.5 ka.

DISCUSSION

Landscape evolution

The formation of the RB site is related to gravitational processes acting on the Paret de l´Ós cliff, whose development was itself driven by the fluvial downcutting of a Segre incised meander. This meander is characterized by low terraces at its southern margin and the vertical cliff and a talus slope at its northern margin, indicating a preferential lateral migration of the river towards the outer bank. The cliff reaches a relative height of about + 145 m above the modern Segre River, indicating that the initial formation of the cliff would have taken place in the last stages of the early Pleistocene, if we consider the ESR ages (1276 ka and 817 ka) available for Alcanadre River terraces lying at + 180–200 m and + 120 m, respectively (Duval et al., 2015). Mean incision rates for the Alcanadre River during the early Pleistocene are proposed to have been between 0.15 and 0.12 m·ka^{-1} (Sancho et al., 2016). Nevertheless, the available ages of fluvial terraces in the Segre valley indicate a more rapid fluvial downcutting during the middle and late Pleistocene. In particular, ^{10}Be exposure ages for the Segre terraces (Stange et al., 2013b) imply incision rates between 0.54 and 0.76 m·ka^{-1} for the final middle–late Pleistocene. Although the ^{10}Be exposure ages have relatively large dating uncertainties (Stange et al., 2013b), the OSL ages provided by Lewiset al. (2009, 2017) for the Cinca River terraces also indicate late Pleistocene to Holocene high incision rates of 0.38–0.76 m·ka^{-1} for the upper reach and 0.20–0.61 m·ka^{-1} for the lower reach. In the Noguera-Pallaresa River, the terrace at + 15–25 m has been OSL dated by Roqué et al. (2013) to around 23 ka and provides higher incision rates of around 0.87 m·ka^{-1}. Nevertheless, these incision rates documented in the Segre catchment are significantly higher than those obtained from the Gállego River, estimated between 0.16 and 0.39 m·ka^{-1} from the final middle Pleistocene and during the late Pleistocene (Benito et al., 2010).

Incision rates for the Segre valley imply a significant velocity change in landscape, which would have modified the valley and affected access to lithic resources transported by the river (quartzite gravels, Roy Sunyer et al., 2017) during the Neanderthal occupations of the RB site. It has been proposed that at the northern margin of the meander, the lower part of the talus slope is older than the fluvial terrace TQ17 (Jordá Pardo et al., 1994), since gravitational sediments lie on a fluvial bar of terrace TQ18 (Figs. 2 and 3). This could imply that terrace TQ19 is older than the RB site. In this preliminary model, the talus slope would have been developed from the old TQ20 floodplain, and the floodplain resources (water, quartzites, and food) would be located about 17 m below the site during its occupation. However, TQ21 fluvial sediments also have interlayered gravitational blocks and debris deposits, implying that the lower talus slope was active during the formation of TQ22. Slope deposits associated with this terrace have also been described in the Noguera Pallaresa River (Roque et al., 2013).

In order to estimate the landscape valley evolution and the terrace chronologies around the RB site, we calculated a Segre age-incision model (Fig. 7A). These modelled elevation curves represent the general position of the river through time, separating the phreatic zone, located below the curves, from the vadose area, situated above the curves (Fig. 7A). From the age-incision model plot, it can be seen that the RB sediments lie in the interzone defined by the curves of the maximum and minimum terrace tread relative elevation (Fig. 7A), indicating that the Segre River level could have been very near to the site during its formation. Maximum tread relative elevation curves seem to be an overestimation of the age-incision model for this meander, since the RB stratigraphic layers are located below the curve but do not show any fluvial or phreatic features. Instead, the sediments consist mainly of loose breccias of angular clasts with scarce matrix, generated primarily by gravitational processes, which could not have developed in the zone below the river level. On the other hand, minimum tread relative elevation curves are more feasible, indicating that the Segre River would only have been 4 m below the older excavated levels (Fig. 7A). The age-incision model based on the available ^{10}Be ages also reveals that terrace TQ23 would be younger (around 36–37 ka) than the site, which would have formed just after TQ24, when the position of the river was less incised and vertically very close to the site. Additionally, this position would imply that floodplain resources would have been found near the site during the late Pleistocene human occupation period, but the site elevation would not have provided a significant strategic 'lookout' across the valley. According to these models, the mean river incision rate during the occupation of the site would have been around 0.5 m·ka^{-1}, which is within the range of incision rates described for other Segre tributaries. Nevertheless, it would be worthwhile undertaking additional dating of associated deposits in the future to corroborate these models, since there are still significant discrepancies between similar terraces in the sequences of the Segre and Gállego catchments. In other Segre tributaries, terrace levels with a similar relative elevation to Segre TQ25 have yielded very young OSL ages in the Noguera-Pallaresa River (20–25 ka, Roqué et al., 2013), older OSL ages in the Cinca River (47 ka, with outliers at 39 and 79 ka, Lewis et al., 2009, 2017), and much older ages in the Gállego River (110–124 ka, Benito et al., 2010).

The geomorphic and stratigraphic evidence suggests that the talus slope formation could have been complex and prolonged during different phases of valley incision. The investigation of the talus slope geometry through ERT has also revealed a heterogeneous underground profile, which is consistent with a complex formation history. The talus slope

transversal geometry shows a projection structure defined by bedrock resistivity (rock projection [RP] structure, Fig. 4, Profiles 1, 5, and 6), which is located between the upper and lower part of the talus slope. Although this ERT structure could be interpreted as being detached from the bedrock to the west (RP structure, Fig. 4, Profile 1), in the profile located just below the RB excavation it appears to be connected to the bedrock (RP structure, Fig. 4, Profile 6). Therefore, beneath the site, this structure can be interpreted as a rocky projection that separates two different sedimentary accommodation spaces in the talus slope, defined by an upper concave-up space (UCS structure, Fig. 4, Profiles 1, 5, and 6) and the lower part of the talus slope. These two spaces show different structures and positions that could have operated in different times during the valley incision.

The concave-up shape of the UCS structure would explain the N–S concave-up layer structure identified during the excavation (Benito-Calvo et al., 2009). This concave structure of the bedrock could have been generated by fluvio-karstic processes undermining the cliff, probably during the abandonment of the TQ26 paleofloodplain, tentatively in the transition from MIS4 to MIS3 (Fig. 7A). As with the scarps described in karstic soluble sediments of the Ebro basin evaporitic formations (Guerrero and Gutiérrez, 2017), undermining by the lateral migration of the river leads to vertical and overhanging unstable slopes, which induce gravitational processes, as preserved in the RB sequence. The latter is composed mainly of clast-supported breccias, consisting of limestone and conglomerate angular clasts of autochthonous origin and sourced from the cliff itself. These sedimentological characteristics reveal that the main depositional processes would have been related to heterogeneous rockfall processes (layers RB-M, RB-H, and RB-F, Fig. 5) triggered by freeze–thaw, frost-cracking, pressure release, weathering, or extreme precipitation events on the cliff (Luckman, 2013) and favored by the discontinuities of the bedrock, such as fractures or the lithological contact between the Eocene limestones and Oligocene conglomerates. However, sorting processes such as dry grain flow or slope wash could also have occurred, as indicated by the local presence in the RB sequence of stratified slope deposits of scarce matrix (layers RB-Q, RB-P, RB-R, and western RB-N, Fig. 5), which are usually related to such mechanisms (Bertran and Texier, 1999; Van Steijn, 2011).

Local sorting processes do not seem to have significantly affected the archaeological assemblages. The preservation of abundant combustion structures (Mora et al., 2014; Martínez-Moreno et al., 2016) and the different patterns shown by fabric artifacts and natural clasts (Benito-Calvo et al., 2009) suggest only scarce post-depositional rearrangement of the excavated archaeological surfaces. Rockfall and stratified slope deposits are commonly associated with cold conditions in periglacial and mountain environments. Nevertheless, similar sedimentological characteristics have also been described in temperate upland environments (García-Ruiz et al., 2001; Van Steijn, 2011), and aggradation on slopes located to the north of the study area have been related to vegetation cover and humidity conditions (Roqué et al., 2013). There is some evidence in the RB sequence to suggest that a non-extreme cold climate prevailed during the site formation period, namely: (1) the site is located at a low altitude (278 m asl), (2) the rock shelter has a southern orientation with a high insolation degree, and (3) the sequence is capped by a flowstone unit, denoting the existence of warm and wet conditions at the top of the sequence. The OSL ages obtained from RB layers indicate formation of the site during the MIS3 interstadial (Fig. 7A). However, this interstadial was also characterized by several abrupt climatic changes, such as the Dansgaard-Oeschger warming episodes and cold Heinrich events.

Closer comparison of the RB chronostratigraphic sequence with marine isotope climatic curves (Svensson et al., 2008; Rasmussen et al., 2014) also suggests that sedimentation of the site may have coincided with colder phases that occurred between interstadials within MIS3 (Fig. 7B), in a manner similar to other stratified screes (Peña Monné et al., 2018). The RB-O stratigraphic unit and the top of RB-Q include sandy layers, locally laminated, which imply overland flows (Bertran and Texier, 1999) related to warmer conditions, as inferred from the concentration of pedogenetic carbonated laminar concretions in RB-O. The sedimentation rates show an increasing trend from the base to the top of the excavated sequence (Fig. 7B), defined by rates of 0.16 $m \cdot ka^{-1}$ from RB-G to RB-M, and 0.44 $m \cdot ka^{-1}$ from RB-M to RB-N and from RB-N to RB-O. The sedimentation of the RB sequence coincides with a phase of slope aggradation proposed in the main basins of Spain, which spans 55.2–47.4 ka (Gutiérrez et al., 2010).

After the RB sedimentary layers accumulated, the Segre River continued to extend downslope by incision, seemingly leaving some fluvial sediments as remnant deposits attached to the slope. So far, no stratigraphical or chronological data is available to establish the relationship between the top of the RB site and the fluvial evolution of the Segre meander, but it is feasible that the last stages recorded at the top of the talus slope formed when terrace TQ27 was deposited, since gravitational deposits are found in and on TQ28. At a similar terrace level (about + 20 m above the Segre), a distinctive phase of slope aggradation has been documented in the Tremp depression, and its formation has been explained as relating to a period of higher humidity and vegetation cover (Roqué et al., 2013). The highest humidity conditions in the RB sequence could be related to the precipitation of the flowstones, whose source is related to seepages within the cliff. Carbonate-rich water seepage during wet events would have produced the flowstone concretion coating the cliff and formed the sub-horizontal flowstone units at the talus slope surface. The sub-horizontal flowstone unit marks the old paleotopography of the talus slope top, which dips locally 8° towards the southwest. Presently, the existence of an upper flowstone sub-horizontal layer hanging on the cliff and detached from the talus slope demonstrates a higher past elevation for the talus slope than the current position. This evidence suggests that the talus slope was subjected to

erosional processes during its final accumulation stages, which modified its original morphology accordingly.

Archaeological implications

In recent years, it has been proposed that the Iberian Peninsula was an ecological "refuge" in which Neanderthals remained in southern Iberia until MIS2 (Finlayson et al., 2006), although there is currently no clear consensus on this issue (see, among others, Zilhão, 2009). Additionally, the cycles and climatic crises that have taken place during MIS3 are considered to have been an active agent in Neanderthal extinction (Jimenez-Espejo et al., 2007). Although the impact of these events is not easy to identify, it has been proposed that MIS3 climatic oscillations determined Neanderthal presence in the southernmost ranges of the Pre-Pyrenees. According to this model, phases of certain climatic stability such as the Greenland Interstadial phases would have sustained an ecosystem compatible with Neanderthal subsistence. Conversely, marine core records indicate that stadial events and Heinrich events could have been associated with significant drops in temperatures and arid conditions in northeast Iberia, which would have promoted the expansion of semi-desertic landscapes (d'Errico and Sanchez Goñi, 2003). Ice and marine core proxy simulations of Heinrich 4 confirm the occurrence of such cold conditions regionally and suggest that periods of extreme aridity are extendable to other stadial phases (Greenland stadials [GS]) of MIS3 (Sepulchre et al., 2007). The adverse conditions associated with major climatic variations would have acted to modulate Neanderthal presence in the southern Pre-Pyrenees, with a cyclical reoccupation of those environments taking place during warmer and wetter Greenland interstadial phases. Several Neanderthal sites in the Segre area have been tentatively assigned to MIS3 (de la Torre et al., 2013). However, these sites have limited radiometric records, and the information currently available does not allow detailed evaluation of the impacts of MIS3 climatic variability on Neanderthal occupations or sedimentary dynamics.

At the RB site, flowstones situated at the top are indicative of higher humidity phases and the last stages of the talus slope development. Although pollen is not preserved at RB, this interpretation could be consistent with the predominance of black pine forest (*Pinus sylvestris*) at Cova Gran, a site close to RB (Allué et al., 2018). Anthraco-analysis of cryophilous pine woodlands indicates the prevalence of supra-Mediterranean conditions with medium average temperatures ranging between 8 and 13°C during the late Pleistocene (Vidal Matutano, 2018). At the same time, throughout the archaeological sequence of the RB site, hackberry seeds (*Celtis australis*), a proxy of mixed forests with hydrophilic requirements characteristic of temperate climates, are detected. The presence of this taxon is recurrent throughout the Pleistocene (see references in Hardy, 2018) and has been noted in other MIS3 Mediterranean Mousterian sites of Iberia (Vidal-Matutano et al., 2018). While the deficient conservation of faunal remains at the RB site hinders detailed paleoecological inferences, we have recovered species related to arid prairie environments, such as *Equus sp. asinus/hydruntinus* and *Stephanorhinus* sp., which are found in association with *Cervus elaphus*, *Bos* sp., *Equus ferus*, *Capra pyrenaica,* and tortoise. This assemblage of eurytherm macro-mammals reflects a mosaic landscape that combined grasslands and forested areas. Thus, although these paleoecological indicators are limited, they do not necessarily support the occurrence of generalized extreme environmental conditions, as otherwise indicated by climate models that sustain the notion that an MIS3 environmental crisis played an active role in Neanderthal demise (Jiménez-Espejo et al., 2007).

In order to better evaluate the impact of MIS3 stadial/interstadial climate fluctuations, it is essential to have more extensive and more precise chronometric records of Neanderthal occupations regionally. There are still major chronological uncertainties that prevent reliable evaluations of possible Neanderthal survival across various areas of the Iberian Peninsula (Finlayson et al., 2006; García Garriga et al., 2012). With reference to northeast Iberia, the model of Neanderthal occupation is based on: (1) a scarce number of individual ages, (2) insufficient evaluations of the stratigraphic relationship between dating samples and the archaeological record, and (3) lack of consideration of dating quality or methodological suitability in discussions of Neanderthal demise and, more generally, the Middle to Upper Paleolithic "transition" (Mora et al., 2018). The latter consideration is particularly significant as the application of new accelerator mass spectrometry (AMS) ^{14}C sample treatment protocols has cast doubt on previously generated chronologies for the "late" Middle Paleolithic (Wood et al., 2013).

At RB, the ^{14}C results obtained previously on bone samples are variously affected by problems related to the low quality of collagen, which typically result in ages that are unrealistically young for Neanderthal sites. At the same time, except for one sample, the ^{14}C ages obtained on charcoal exceed the finite dating range of the ^{14}C technique (Table 3; Terradas et al., 1993; Jordá Pardo et al., 1994; Martinez-Moreno et al., 2006). These problems have been detected in other Mousterian sites (Higham et al. 2009; Wood et al. 2013) and warn of the difficulty of deriving reliable bone or charcoal ^{14}C records for the period spanning 50–30 ka (Wood, 2015).

The five new OSL ages obtained for RB in this study provide a much firmer chronometric framework for the Mousterian occupations of the site (Table 2). The ages obtained from sedimentary layers RB-G (archaeological level S9), RB-M (archaeological level N14), RB-N (archaeological level N12), and RB-O, are stratigraphically coherent and overlap with each other at their 1σ uncertainty ranges. According to these new ages, archaeological level S9 could tentatively be aligned with climatic event GS-15 around 55 ka (INTIMATE group, INTegration of Ice-core, MArine and TErrestrial records, Rasmussen et al., 2014), and archaeological levels N14 and N12 could be in GS-13, with mean chronological ages of 48.4–48.8 ka; however, these interpretations are partially limited by the size of the associated OSL uncertainty

Table 3. Charcoal and bone series accelerator mass spectrometry ^{14}C ages from Roca dels Bous.

Level	Lab #[a]	^{14}C yr BP	^{14}C procedure[b]	Sample	Remarks	Reference
R3	AA-6481	38800 +/− 1200	AMS	Isolated charcoal		Terradas et al. 1993
S1	AA-6480	> 46900	AMS	Isolated charcoal	Out of range	
R3	Ua-21493	18110 +/− 170	AMS	Isolated bone	Light burned bone	Martínez-Moreno et al. 2006
N10	Ua-21494	16515 +/− 145	AMS	Isolated bone	Light burned bone	
N10	Ua-21899	> 43000	AMS	Isolated charcoal	Out of range	
R8	Ua-sn			Isolated bone	Not treated due to technical problems (without collagen)	
N10	Ua-sn			Isolated bone	Unburned bone without collagen	
S1	Ua-sn			Isolated bone	Unburned bone without collagen	

[a]AA corresponds to Arizona Radiocarbon Laboratory, Ua to Uppsala Radiocarbon Laboratory
[b]AMS is accelerator mass spectrometry

ranges. Following this chronostratigraphic sequence, archaeological level N10 (layer RB-R) could potentially be related to GS-12b/c, between 48 and 47 ka. The OSL ages collectively suggest that RB records a succession of multiple Neanderthal occupations spanning a relatively short time range, in which significant climatic changes are known to have occurred and which could have potentially affected the ecosystems of the area.

Such ecosystem changes could be reflected in the configuration of the artifacts observed in the different archaeological levels (Martínez-Moreno et al., 2004). Although N10 and N12 correspond to a similar organizational pattern, their lithic assemblages are structured towards high residential mobility and appear to correspond with short occupation events aimed at the exploitation of resources adjacent to the site. However, variations in the composition of lithic instruments and, in particular, the collection of raw materials, especially the high presence of metamorphic rocks found in the river system (terraces or in the river), is interesting (Roy Sunyer et al., 2017). Although our landscape reconstruction indicates the river position was close and this raw material type was readily available, the archaeological observations reveal important differences for these two occupation horizons. In archaeological level N12 (>22,000 lithic artifacts), 85% of the lithic artifacts are made of quartzite, while in lN10 (2,000 artifacts), only 28% consist of quartzite. The rest of the material corresponds to various types of flint, which were brought to the site from distances of between 10 and 25 km (Roy Sunyer, 2016). These changes in the use of raw material over time are paralleled by transformations in the lithic size systems and in the morphology of the retouched tools. In level N12, the type of knapping method used was essentially the Levallois system, while in N10 the knapping methods were more expeditious. Moreover, significant differences in configuration, morphology, and intensity of formal artifact use are apparent, which indicate a progressive tool kit miniaturization on retouched flint pieces, especially in level N10 (Mora et al., 2004). The OSL dating results for the RB sequence indicate that these changes in lithic assemblages occurred over a relatively short time scale (i.e., over timescales that cannot be differentiated beyond the existing OSL uncertainty ranges) and under potentially different climatic conditions related to alternating warm and cold stages within MIS3. The implications of these findings are significant and require further examination in the future, since the temporal trends of raw material collection and lithic artifact management show a profound remodeling of mobility, settlement pattern, and landscape use by the Neanderthals who visited the RB site (Martínez-Moreno et al., 2010).

Finally, the OSL chronometric ranges indicate that the Mousterian occupations of RB around 48–52 ka are related to the final phases of the biological and cultural history of Neanderthals. In this regard, the previously published finite AMS ^{14}C age obtained on charcoal sample AA-6481 is particularly relevant. This charcoal sample was obtained from Mousterian level R3 (Table 3), which is located above archaeological levels N10, N12, and N14, and yielded a calibrated age of 44.0–42.2 cal ka BP (68% confidence interval; Calpal online 2019), within GS-12. This age estimate for level R3, if considered reliable, would support the general suitability of the OSL ages obtained in this study for levels N12 and N14, and could possibly indicate that the site was not visited during Heinrich Event 5 at ~45 ka. Likewise, the 14C age for R3 suggests that Neanderthals were reinstated in this area at a time close to their disappearance from Western Europe, which has been established as occurring at 40.8–40 cal ka BP (1σ) (Higham et al., 2014).

CONCLUSIONS

Using a multidisciplinary approach that combines geomorphological studies (LIDAR data and UAV surveys), stratigraphical descriptions, new geochronological datasets (OSL dating), statistical methods, and geophysical surveying (ERT), we have reconstructed the landscape evolution of RB. Through this work, we have been able to estimate the original paleogeographical position of this rock shelter in the landscape and the processes, ages, rates, and climatic conditions associated with the site formation.

Our analysis reveals that the cliff hosting the RB rock shelter developed along the outer bank of an asymmetric incised meander, and its geometry evolved from the early Pleistocene onwards as a result of incision and undermining by the Segre River channel. The sedimentation of the rock shelter took place between 47 and 55 ka, in an accommodation space generated by fluvial erosion of the bedrock, probably towards the beginning of MIS3. During the Mousterian settlement of the site, Segre floodplain resources (water and lithic raw material) were likely found at a very similar topographic level to that of the RB site, although additional dating studies of associated fluvial terraces in the region would be advisable to resolve some existing discrepancies between the chronostratigraphic sequences of the South Pyrenees valleys. The main processes involved in the sedimentation of the RB sequence during MIS3 occurred at rates of 0.16–0.44 $m{\cdot}ka^{-1}$ and correspond to rockfall processes and, to a lesser degree, to local sorting processes such as grain flow or slope wash flows that did not significantly affect the stratigraphic integrity of the archaeological assemblage. Comparisons with regional isotopic climatic curves reveal that the RB layers could potentially have been deposited during colder phases occurring between MIS3 interstadials. The RB sedimentary sequence ended with the deposition of an undated flowstone unit related to cliff seepages, which probably imply a higher humidity phase.

Our landscape reconstruction and the generation of a reliable chronometric record have provided much-needed datasets for better understanding the evolution of the environment surrounding RB, which seems to register a significant transformation that affected the Neanderthal lifestyle during MIS3. These new results will permit improved future comparisons of late Pleistocene human occupation dynamics across the southeastern Pre-Pyrenees region, which is a key geographic focus of several debates related to Neanderthal demise in Western Europe.

ACKNOWLEDGMENTS

This study was supported by research projects from the Spanish Government (*Human settlement during the Upper Pleistocene and Holocene in the South-eastern Pyrenees,* HAR2016-75124-P), Generalitat de Catalunya (SGR2017-1357 and SGR2017-836), and Department of Culture Generalitat de Catalunya. Leticia Miguens Rodríguez performed the textural analysis at the Geology Laboratory (CENIEH). Ana Isabel Alvaro Gallo carried out the X-ray diffraction analysis in the Archaeometry laboratory (CENIEH). GIS and 3D mapping were performed using the facilities of the Digital Mapping and 3D Laboratory (CENIEH). LA thanks Carlos Pérez Garrido for his assistance with preparing and measuring the optically stimulated luminescence samples in the CENIEH Luminescence Dating Laboratory. We thank Derek Booth, Curtis W. Marean, Francisco Gutiérrez, and an anonymous reviewer for their helpful comments and inputs.

REFERENCES

Allué, E., Martínez-Moreno, J., Roy, M., Benito-Calvo, A., Mora, R., 2018. Montane pine forests in NE Iberia during MIS 3 and MIS 2. A study based on new anthracological evidence from Cova Gran (Santa Linya, Iberian Pre-Pyrenees). *Review of Palaeobotany and Palynology* 258, 62–72.

Arnold, L.J., Bailey, R.M., Tucker, G.E., 2007. Statistical treatment of fluvial dose distributions from southern Colorado arroyo deposits. *Quaternary Geochronology* 2, 162–167.

Arnold, L.J., Demuro, M.D., 2018. Dating and Optically Stimulated Luminescence. In S.L. López Varela (Ed.), *The Encyclopedia of Archaeological Sciences*. Wiley-Blackwell, New Jersey, USA, pp. 1992.

Arnold, L.J., Demuro, M., Navazo Ruiz, M., 2012b. Empirical insights into multi-grain averaging effects from 'pseudo' single-grain OSL measurements. *Radiation Measurements* 47, 652–658.

Arnold, L.J., Demuro, M., Navazo Ruiz, M., Benito-Calvo, A., Pérez-González, A., 2013. OSL dating of the Middle Palaeolithic Hotel California site, Sierra de Atapuerca, north-central Spain. *Boreas* 42, 285–305.

Arnold, L.J., Demuro, M., Parés, J.M., Arsuaga, J.L., Aranburu, A., Bermúdez de Castro, J.M., Carbonell, E., 2014. Luminescence dating and palaeomagnetic age constraint on hominins from Sima de los Huesos, Atapuerca, Spain. *Journal of Human Evolution* 67, 85–107.

Arnold, L.J., Demuro, M., Parés, J.M., Pérez-González, A., Arsuaga, J.L., Bermúdez de Castro, J.M., Carbonell, E., 2015. Evaluating the suitability of extended-range luminescence dating techniques over early and Middle Pleistocene timescales: Published datasets and case studies from Atapuerca, Spain. *Quaternary International* 389, 167–190.

Arnold, L.J., Duval, M., Demuro, M., Spooner, N.A., Santonja, M., Pérez-González, A., 2016. OSL dating of individual quartz 'supergrainsä from the Ancient Middle Palaeolithic site of Cuesta de la Bajada, Spain. *Quaternary Geochronology* 36, 78–101.

Arnold, L.J., Duval, M., Falguères, C., Bahain, J.-J., Demuro, M. 2012a. Portable gamma spectrometry with cerium-doped lanthanum bromide scintillators: Suitability assessments for luminescence and electron spin resonance dating applications. *Radiation Measurements* 47, 6–18.

Arnold L.J., Roberts, R.G., 2009. Stochastic modelling of multi-grain equivalent dose (D_e) distributions: Implications for OSL dating of sediment mixtures. *Quaternary Geochronology* 4, 204–230.

Arnold, L.J., Roberts, R.G., Galbraith, R.F., DeLong, S.B., 2009. A revised burial dose estimation procedure for optical dating of young and modern-age sediments. *Quaternary Geochronology* 4, 306–325.

Arnold, L. J., Roberts, R. G., MacPhee, R. D. E., Willerslev, E., Tikhonov, A. N., Brock, F., 2008. Optical dating of perennially frozen deposits associated with preserved ancient plant and animal DNA in north-central Siberia. *Quaternary Geochronology* 3, 114–136.

Badía, D., Martí, C., Palacio, E., Sancho, C., Poch, R.M., 2009. Soil evolution over the Quaternary period in a semiarid climate (Segre river terraces, northeast Spain). *Catena* 77, 165–174.

Bailey, G.N., King, G.C.P., 2011. Dynamic landscapes and human dispersal patterns: Tectonics, coastlines, and the reconstruction of human habitats. *Quaternary Science Reviews* 30, 1533–1553.

Bailey, R.M., Arnold, L.J. 2006. Statistical modelling of single grain quartz De distributions and an assessment of procedures for estimating burial dose. *Quaternary Science Reviews* 25, 2475–2502.

Benito-Calvo, A., Martínez-Moreno, J., Jordá Pardo, J.F., de la Torre, I., Mora Torcal, R., 2009. Sedimentological and

archaeological fabrics in Palaeolithic levels of the South-Eastern Pyrenees: Cova Gran and Roca dels Bous Sites (Lleida, Spain). *Journal of Archaeological Science* 36, 2566–2577.

Benito-Calvo, A., Ortega, A.I., Pérez-González, A., Campaña, I., Bermúdez de Castro, J.M., Carbonell, E., 2017. Palaeogeographical reconstruction of the Sierra de Atapuerca Pleistocene sites (Burgos, Spain). *Quaternary International* 433, 379–392.

Benito-Calvo, A., A. Pérez-González, Parés, J.M., 2008. Quantitative reconstruction of Late Cenozoic landscapes: A case study in the Sierra de Atapuerca (Burgos, Spain). *Earth Surface Processes and Landforms* 33, 2 (2008): 196–208.

Benito, G., Sancho, C., Peña, J.L., Machado, M.J., Rhodes, E.J., 2010. Large-scale karst subsidence and accelerated fluvial aggradation during MIS6 in NE Spain: climatic and paleohydrological implications. *Quaternary Science Reviews* 29, 2694–2704.

Bertran, P., Texier, J.-P., 1999. Sedimentation processes and facies on a semi-vegetated talus, Lousteau, Southwestern France. *Earth Surface Processes and Landforms* 24, 177–187.

Bøtter-Jensen, L., Mejdahl, M., 1988. Assessment of beta dose-rate using a GM multicounter system. *Nuclear Tracks and Radiation Measurements* 14, 187–191.

Bowler, J.M., Johnston, H., Olley, J.M., Prescott, J.R., Roberts, R.G., Shawcross, W., Spooner, N.A., 2003. New ages for human occupation and climate change at Lake Mungo, Australia. *Nature* 421, 837–840.

Brennan, B.J., 2003. Beta doses to spherical grains. *Radiation Measurements* 37, 299–303.

Calpal online, 2019. Cologne Radiocarbon Calibration & Paleoclimate Research Package: Calpal online (accessed 4.20.19). http://www.calpal-online.de/.

Confederación Hidrográfica del Ebro, 2019. Confederación Hidrográfica del Ebro (accessed 4.20.19). http://www.chebro.es/.

de la Torre, I., Martínez-Moreno, J., Mora, R., 2013. Change and Stasis in the Iberian Middle Paleolithic: Considerations on the Significance of Mousterian Technological Variability. *Current Anthropology* 54, S320–S336.

Demuro, M., Arnold, L.J., Aranburu, A., Gómez-Olivencia, A., Arsuaga, J.L., 2019b. Single-grain OSL dating of the Middle Palaeolithic site of Galería de las Estatuas, Atapuerca (Burgos, Spain) *Quaternary Geochronology* 49, 138–145.

Demuro, M., Arnold, L.J., Aranburu, A., Sala, N., Arsuaga, J.-L., 2019a. New bracketing luminescence ages constrain the Sima de los Huesos hominin fossils (Atapuerca, Spain) to MIS 12. *Journal of Human Evolution* 131, 76–95.

Demuro, M., Arnold, L.J., Froese, D.G., Roberts, R.G., 2013. OSL dating of loess deposits bracketing Sheep Creek tephra beds, northwest Canada: Dim and problematic single-grain OSL characteristics and their effect on multi-grain age estimates. *Quaternary Geochronology* 15, 67–87.

d'Errico, F., Sánchez Goñi, M.F., 2003. Neandertal extinction and the millennial scale climatic variability of OIS 3. *Quaternary Science Reviews* 22, 769–788.

Duller, G.A.T., 2008. *Luminescence Dating: Guidelines on using luminescence dating in archaeology*. English Heritage, Swindon.

Duval, M., Sancho, C., Calle, M., Guilarte, V., Peña-Monné, J.L., 2015. On the interest of using the multiple center approach in ESR dating of optically bleached quartz grains: Some examples from the Early Pleistocene terraces of the Alcanadre River (Ebro basin, Spain). *Quaternary Geochronology* 29, 58–69.

Finlayson, C., Giles Pacheco, F., Rodríguez-Vidal, J., Fa, D.A., Gutierrez López, J.M., Santiago Pérez, A., Finlayson, G., *et al.*, 2006. Late survival of Neanderthals at the southernmost extreme of Europe. *Nature* 443, 850–853.

Galbraith, R.F., Roberts, R.G., Laslett, G.M., Yoshida, H., Olley, J.M., 1999. Optical dating of single and multiple grains of quartz from Jinmium rock shelter, northern Australia: Part I, Experimental design and statistical models. *Archaeometry* 41, 339–364.

García-Ruiz, J.M., Valero-Garcés, B., González-Sampériz, P., Lorente, A., Martí-Bono, C., Beguería, S., Edwards, L., 2001. Stratified scree in the Central Spanish Pyrenees: Palaeoenvironmental implications. *Permafrost and Periglacial Processes* 12, 233–242.

García Garriga, J., Martínez Molina, K., Baena Preysler, J., 2012. Neanderthal Survival in the North of the Iberian Peninsula? Reflections from a Catalan and Cantabrian Perspective. *Journal of World Prehistory* 25, 81–121.

Guérin, G., Mercier, N., Adamiec, G., 2011. Dose-rate conversion factors: Update. *Ancient TL* 29, 5–8.

Guerrero, J., Gutiérrez, F., 2017. Gypsum scarps and asymmetric fluvial valleys in evaporitic terrains. The role of river migration, landslides, karstification and lithology (Ebro River, NE Spain). *Geomorphology* 297, 137–152.

Gutiérrez, M., Lucha, P., Gutiérrez, F., Moreno, A., Guerrero, J., Martín-Serrano, A., Nozal, F., Desir, G., Marin, C., Bonachea, J., 2010. Are talus flatiron sequences in Spain climate-controlled landforms? *Zeitschrift für Geomorphologie* 54, 243–252.

Hardy, K., 2018. Plant use in the Lower and Middle Palaeolithic: Food, medicine, and raw materials. *Quaternary Science Reviews* 191, 393–405.

Higham, T., Brock, F., Peresani, M., Broglio, A., Wood, R., Douka, K. 2009. Problems with radiocarbon dating the Middle to Upper Palaeolithic transition in Italy. *Quaternary Science Reviews* 28, 1257–1267.

Higham, T., Douka, K., Wood, R., Ramsey, C.B., Brock, F., Basell, L., Camps, M., *et al.*, 2014. The timing and spatiotemporal patterning of Neanderthal disappearance. *Nature* 512, 306–209.

Jacobs, Z., Duller, G.A.T., Wintle, A.G., 2006. Interpretation of single-grain D_e distributions and calculation of D_e. *Radiation Measurements* 41, 264–277.

Jiménez-Espejo, F.J., Martínez-Ruiz, F., Finlayson, C., Paytan, A., Sakamoto, T., Ortega-Huertas, M., Finlayson, G., Iijima, K., Gallego-Torres, D., Fa, D., 2007. Climate forcing and Neanderthal extinction in Southern Iberia: insights from a multiproxy marine record. *Quaternary Science Reviews* 26, 836–852.

Jordá Pardo, J.F., 2005. El registro arqueológico kárstico durante el Pleistoceno superior final en la vertiente meridional de los Pirineos: geoarqueología, geodinámica y sedimentación, in: Cura, M., Sóler, N., Maroto, J. (Eds.), *Praehistoria Pyrenaica. II Congrés Internacional Història dels Pirineus*. Centre Associat de la UNED, pp. 129–159.

Jordá Pardo, J.F., Martínez, J., Mora Torcal, R., Sánchez Casado, F.L., 1994. Modelos deposicionales y ocupación antrópica en el NE de la Península Ibérica durante el Paleolítico Medio, in: Jordá Pardo, J.F. (Ed.), *Geoarqueología (Actas de La 2^0 Reunión Nacional de Geoarqueología)*. Instituto Tecnológico Geominero de España y Asociación Española para el Estudio del Cuaternario, Madrid, pp. 35–48.

Lazar, M, Schattner, M.L., 2010. Landscape evolution and hominin dispersal. *Quaternary Science Reviews* 29, 1495–1500.

Lewis, C.J., McDonald, E.V., Sancho, C., Peña Monné, J.L., Rhodes, E.J., 2009. Climatic implications of correlated Upper Pleistocene glacial and fluvial deposits on the Cinca and Gállego Rivers (NE Spain) based on OSL dating and soil stratigraphy. *Global and Planetary Change* 67, 141–152.

Lewis, C.J., Sancho, C., McDonald, E.V., Peña Monné, J.L., Pueyo, E.L., Rhodes, E., Calle, M., Soto, R., 2017. Post-tectonic landscape evolution in NE Iberia using staircase terraces: Combined effects of uplift and climate. *Geomorphology* 292, 85–103.

Lisiecki, L.E., Raymo, M.E., 2005. A Pliocene-Pleistocene stack of 57 globally distributed benthic δ18O records. *Paleoceanography* 20, 1–17.

Lucha, P., 2009. Subsidencia por disolución de evaporitas y halocinesis en el anticlinal de Barbastro y el valle del río Cardener (Cuenca Terciaria de. Ebro). Ph.D. dissertation, Universidad de Zaragoza, Zaragoza.

Lucha, P., Gutiérrez, F., Galve, J.P., Guerrero, J., 2012. Geomorphic and stratigraphic evidence of incision-induced halokinetic uplift and dissolution subsidence in transverse drainages crossing the evaporite-cored Barbastro-Balaguer Anticline (Ebro Basin, NE Spain). *Geomorphology* 171–172, 154–172.

Luckman, B.H., 2013. Processes, Transport, Deposition, and Landforms: Rockfall. In: *Treatise on Geomorphology*. Vol. 7, Elsevier Academic Press, pp. 174–182.

Martínez-Moreno, J., de la Torre, I., Mora, R., Casanova, J., 2010. Technical variability and change in the pattern of settlement at Roca dels Bous (southeastern Pre-Pyrenees, Spain). In: Conard, N.J., Delagnes, A. (Eds.), *Settlement Dynamics of the Middle Paleolithic and Middle Stone Age*. Vol. III, Kerns Verlag, Tubingen, pp. 485–507.

Martínez-Moreno, J., Mora, R., de la Torre, I., 2004. Methodological approach for understanding Middle Palaeolithic settlement dynamics at la Roca dels Bous. In Conard, N. (Ed.), *Settlement Dynamics of the Middle Paleolithic and Middle Stone Age*. Vol. II, Kerns Verlag, Tübingen, pp. 393–413.

Martínez-Moreno, J, Mora Torcal, R., de la Torre, I., 2006. La Roca dels Bous en el contexto del Paleolítico Medio final del Noreste de la Península Ibérica. *Zona Arqueológica,* Miscelánea en homenaje a Victoria Cabrera 7, 253–262.

Martínez-Moreno, J., Mora Torcal, R., Roy Sunyer, M., Benito-Calvo, A., 2016. From site formation processes to human behaviour: Towards a constructive approach to depict palimpsests in Roca dels Bous. *Quaternary International* 417, 82–93.

Mayya, Y.S., Morthekai, P., Murari, M.K., Singhvi, A.K., 2006. Towards quantifying beta microdosimetric effects in single-grain quartz dose distribution. *Radiation Measurements* 41, 1032–1039.

Mejdahl, V., 1979. Thermoluminescence dating: beta-dose attenuation in quartz grains. *Archaeometry* 21, 61–72.

Mejdahl, V., 1987. Internal radioactivity in quartz and feldspar grains. *Ancient TL* 5, 10–17.

Mora, R., Benito-Calvo, A., Martínez-Moreno, J., Marcén, P.G., de La Torre, I., 2011. Chrono-stratigraphy of the Upper Pleistocene and Holocene archaeological sequence in Cova Gran (southeastern Pre-Pyrenees, Iberian Peninsula). *Journal of Quaternary Science* 26, 635–644.

Mora, R., de la Torre, I., Martínez-Moreno, J., 2004. Middle Palaeolithic mobility and land use in the Southwestern Pyrenees: The example of level 10 in la Roca dels Bous (Noguera, Catalunya, Northeast Spain). In: Conard, N. (Ed.), *Settlement Dynamics of the Middle Paleolithic and Middle Stone Age*. Vol. II, Kerns Verlag, Tübingen, pp. 415–435.

Mora, R., Martínez-Moreno, J., Roda, X., de la Torre, I., Benito Calvo, A., Roy, M., Samper Carro, S., Bolívar, S., Pizarro, J., Plasencia, J., 2014. The Mousterian site of Roca dels Bous (Lleida, Pre-pyrenees). In: Salas Ramos, R. (Ed.), *Pleistocene and Holocene Hunter-Gatherers in Iberia and the Gibraltar Strait: The Current Archaeological Record*. Burgos, pp. 159–162.

Mora, R., Martínez-Moreno, J., Roy Sunyer, M., Benito Calvo, A., Polo-Díaz, A., Samper Carro, S., 2018. Contextual, technological and chronometric data from Cova Gran: Their contribution to discussion of the Middle-to-Upper Paleolithic transition in northeastern Iberia. *Quaternary International* 474, 30–43.

Murray, A.S., Wintle, A., 2000. Luminescence dating of quartz using an improved single-aliquot regenerative-dose protocol. *Radiation Measurements* 32, 57–73.

Nathan, R.P., Thomas, P.J., Jain, M., Murray, A.S., Rhodes, E.J., 2003. Environmental dose rate heterogeneity of beta radiation and its implications for luminescence dating: Monte Carlo modelling and experimental validation. *Radiation Measurements* 37, 305–313.

Olley, J.M., Caitcheon, G.G., Roberts, R.G., 1999. The origin of dose distributions in fluvial sediments, and the prospect of dating single grains of quartz from fluvial deposits using optically stimulated luminescence. *Radiation Measurements* 30, 207–217.

Olley, J.M., Pietsch, T., Roberts, R.G., 2004. Optical dating of Holocene sediments from a variety of geomorphic settings using single grains of quartz. *Geomorphology* 60, 337–358.

Ortega, A.I., Benito-Calvo, A., Porres, J., Pérez-González, A., Martín Merino, M.A., 2010. Applying electrical resistivity tomography to the identification of endokarstic geometries in the Pleistocene Sites of the Sierra de Atapuerca (Burgos, Spain). *Archaeological Prospection* 17, 233–245.

Pawley, S.M., Bailey, R.M., Rose, J., Moorlock, B.S.P., Hamblin, R.J.O., Booth, S.J., Lee, J.R., 2008. Age limits on Middle Pleistocene glacial sediments from OSL dating, north Norfolk, UK. *Quaternary Science Reviews* 27, 1363–1377.

Peña Monné, J.L., 1983. *La Conca de Tremp y Sierras Prepirenaicas comprendidas entre los Ríos Segre y Noguera Ribagorzana: Estudio geomorfológico*. Instituto de Estudios Ilerdenses, Lérida.

Peña Monné, J.L., Pérez Alberti, A., Sampietro Vattuone, M.M., Otero, X.L., Sánchez Fabre, M., Longares Aladrén, L.A., 2018. The Holocene stratified screes from Sierra de Albarracín (Iberian Ranges, Spain) and their paleoenvironmental significance. *Holocene* 28, 478–491.

Peña Monné, J.L., Sancho Marcen, C., 1988. Correlación y evolución cuaternaria del sistema fluvial Segre-Cinca en su curso bajo. *Cuaternario y Geomorfología* 2, 77–83.

Pocovi, A., Millán, H., Pueyo, E., Larrasoaña, J.C., Oliva, B., 2004. Estructura del frente surpirenaico. In: Vera, J.A. (Ed.), *Geología de España*. Sociedad Geológica de España, IGME, Madrid, pp. 328–330.

Prescott, J.R., Hutton, J.T., 1994. Cosmic ray contributions to dose rates for luminescence and ESR dating: Large depths and long-term time variations. *Radiation Measurements* 23, 497–500.

Rasmussen, S.O., Bigler, M., Blockley, S.P., Blunier, T., Buchardt, S.L., Clausen, H.B., Cvijanovic, I., *et al*. 2014. A stratigraphic framework for abrupt climatic changes during the Last Glacial period based on three synchronized Greenland ice-core records: refining and extending the INTIMATE event stratigraphy. *Quaternary Science Reviews* 106, 14–28.

Rees-Jones, J., 1995. Optical dating of young sediments using fine-grain quartz. *Ancient TL* 13, 9–14.

Rees-Jones, J., Tite, M.S., 1997. Optical dating results for British archaeological sediments. *Archaeometry* 39, 177–187.

Reynolds, S.C., Bailey, G.N., King, G.C.P., 2011. Landscapes and their relation to hominin habitats: Case studies from

Australopithecus sites in eastern and southern Africa. *Journal of Human Evolution* 60, 281–298.

Roberts, R., Bird, M., Olley, J., Galbraith, R., Lawson, E., Laslett, G., Yoshida, H., *et al*., 1998. Optical and radiocarbon dating at Jinmium rock shelter in northern Australia. *Nature* 393, 358–362.

Roqué, C., Linares, R., Zarroca, M., Rosell, J., Pellicer, X.M., Gutiérrez, F., 2013. Chronology and paleoenvironmental interpretation of talus flatiron sequences in a sub-humid mountainous area: Tremp Depression, Spanish Pyrenees. *Earth Surface Processes and Landforms* 38, 1513–1522.

Roy Sunyer, M., 2016. *Materias primas líticas y su explotación durante la prehistoria en el prepirineo oriental (NE de Iberia)*. Ph.D. dissertation, Universitat Autònoma de Barcelona, Barcelona.

Roy Sunyer, M., Mora Torcal, R., Plasencia Figueroa, Fco. J., Martínez-Moreno, J., Benito-Calvo, A., 2017. Quartzite selection in fluvial deposits: The N12 level of Roca dels Bous (Middle Palaeolithic, southeastern Pyrenees). *Quaternary International* 435, 49–60.

Sancho, C., Calle, M., Peña-Monné, J.L., Duval, M., Oliva-Urcia, B., Pueyo, E.L., Benito, G., Moreno, A., 2016. Dating the Earliest Pleistocene alluvial terrace of the Alcanadre River (Ebro Basin, NE Spain): Insights into the landscape evolution and involved processes. *Quaternary International* 407, 86–95.

Saula i Briansó, E., Samsó Escolà, J.M., Escuer Solé, J., Casanovas Petanas, J., 2017. Mapa Geológico de España. E 1:50.000, Hoja n° 328 (Artesa de Segre), Serie Magna. IGME, Madrid.

Sepulchre, P., Ramstein, G., Kageyama, M., Vanhaeren, M., Krinner, G., Sánchez-Goñi, M.-F., d'Errico, F., 2007. H4 abrupt event and late Neanderthal presence in Iberia. *Earth and Planetary Science Letters* 258, 283–292.

Silva, P.G., Roquero, E., López-Recio, M., Huerta, P., Martínez-Graña, A.M., 2016. Chronology of fluvial terrace sequences for large Atlantic rivers in the Iberian Peninsula (Upper Tagus and Duero drainage basins, Central Spain). *Quaternary Science Reviews*. DOI: 10.1016/j.quascirev.2016.05.027.

Silva, P.G., Roquero, E., López-Recio, M., Huerta, P., Tapias, F., 2013. Statistical approach to the chronosequence of fluvial terraces in the Tagus and Duero Basins (Central Spain). In: Baena, R., Fernández, J.J., Guerrero, I. (Eds.), *El Cuaternario Ibérico: Investigación En El S. XXI, VIII Reunión de Cuaternario Ibérico, Sevilla-La Rinconada*. AEQUA, Camas, Sevilla, pp. 29–33.

Stange, K.M., van Balen, R., Carcaillet, J., Vandenberghe, J., 2013a. Terrace staircase development in the Southern Pyrenees Foreland: Inferences from ^{10}Be terrace exposure ages at the Segre River. *Global and Planetary Change* 101, 97–112.

Stange, K.M., van Balen, R., Vandenberghe, J., Peña, J.L., Sancho, C., 2013b. External controls on Quaternary fluvial incision and terrace formation at the Segre River, Southern Pyrenees. *Tectonophysics* 602, 316–331.

Svensson, A., Andersen, K.K., Bigler, M., Clausen, H.B., Dahl-Jensen, D., Davies, S.M., Johnsen, *et al*., 2008. A 60 000 year Greenland stratigraphic ice core chronology. *Climate of the Past* 4, 47–57.

Terradas, X., Mora, R., Martínez, J., Casellas, S., 1993. La Roca dels Bous en el contexto de la transición Paleolítico Medio-Superior en el NE de la Península Ibérica. Cabrera, V. (ed.): *El origen del hombre moderno en el suroeste de Europa*: 247–257. UNED.

Van Steijn, H., 2011. Stratified slope deposits: Periglacial and other processes involved. *Geological Society London Special Publication* 342, 213–226.

Vidal-Matutano, P., 2018. Anthracological data from Middle Palaeolithic contexts in Iberia: What do we know? *Munibe Antropologia-Arkeologia* 69, 5–20.

Vidal-Matutano, P., Pérez-Jordà, G., Hernández, C.M., Galván, B., 2018. Macrobotanical evidence (wood charcoal and seeds) from the Middle Palaeolithic site of El Salt, Eastern Iberia: Palaeoenvironmental data and plant resources catchment areas. *Journal of Archaeological Science: Reports* 19, 454–464.

Wilson, L., 2011. Raw material economics in their environmental context: An example from the Middle Palaeolithic of southern France. *Geological Society London Special Publications* 352, 163–180.

Wood, R., 2015. From revolution to convention: the past, present and future of radiocarbon dating. *Journal of Archaeological Science* 56, 61–72.

Wood, R.E., Barroso-Ruíz, C., Caparrós, M., Jordá Pardo, J.F., Galván Santos, B., Higham, T.F.G., 2013. Radiocarbon dating casts doubt on the late chronology of the Middle to Upper Palaeolithic transition in southern Iberia. *Proceedings of the National Academy of Sciences of the United States of America* 110, 2781–2786.

Zilhão, J., 2009. The Ebro frontier revisited. In: Camps, M., Szmidt, C. (Eds.) *The Mediterranean from 50.000 to 25.000 BP : turning points and new directions*. Oxbow Books, Oxford, pp. 293–312.